0026-895X/01/6006-1210–1225$3.00
MOLECULAR PHARMACOLOGY
Copyright © 2001 The American Society for Pharmacology and Experimental Therapeutics
Mol Pharmacol 60:1210–1225, 2001

Vol. 60, No. 6
961/944471
Printed in U.S.A.

MOL PHARM

Distinct Interaction of Human and Guinea Pig Histamine H_2-Receptor with Guanidine-Type Agonists

MELISSA T. KELLEY,[1] TILMANN BÜRCKSTÜMMER, KATHARINA WENZEL-SEIFERT, STEFAN DOVE, ARMIN BUSCHAUER, and ROLAND SEIFERT

Departments of Pharmacology and Toxicology (M.T.K., K.W.-S., R.S.) and Molecular Biosciences (T.B.), the University of Kansas, Lawrence, Kansas; and Department of Pharmacy, University of Regensburg, Regensburg, Germany (S.D., A.B.)

Received March 16, 2001; accepted July 3, 2001

This paper is available online at http://molpharm.aspetjournals.org

ABSTRACT

It is unknown why the potencies and efficacies of long-chained guanidine-type histamine H_2-receptor (H_2R) agonists are lower at the H_2R of human neutrophils than at the H_2R of the guinea pig atrium. To elucidate these differences, we analyzed fusion proteins of the human H_2R (hH_2R) and guinea pig H_2R (gpH_2R), respectively, and the short splice variant of $G_{s\alpha}$ ($G_{s\alpha S}$) expressed in Sf9 cells. The potencies and efficacies of small H_2R agonists in the GTPase assay and the potencies of antagonists at inhibiting histamine-stimulated GTP hydrolysis by hH_2R-$G_{s\alpha S}$ and gpH_2R-$G_{s\alpha S}$ were similar. In contrast, the potencies and efficacies of guanidines were lower at hH_2R-$G_{s\alpha S}$ than at gpH_2R-$G_{s\alpha S}$. Guanidines bound to hH_2R-$G_{s\alpha S}$ with lower affinity than to gpH_2R-$G_{s\alpha S}$, and high-affinity binding of guanidines at gpH_2R-$G_{s\alpha S}$ was more resistant to disruption by GTPγS than binding at hH_2R-$G_{s\alpha S}$. Molecular modeling suggested that the nonconserved Asp-271 in transmembrane domain 7 of gpH_2R (Ala-271 in hH_2R) confers high potency to guanidines. This hypothesis was confirmed by Ala-271→Asp-271 mutation in hH_2R-$G_{s\alpha S}$. Intriguingly, the efficacies of guanidines at the Ala-271→Asp-271 mutant and at hH_2R/gpH_2R chimeras were lower than at gpH_2R. Our model suggests that a Tyr-17/Asp-271 H-bond, present only in gpH_2R-$G_{s\alpha S}$ but not the other constructs studied, stabilizes the active guanidine-H_2R state. Collectively, our data show 1) distinct interaction of H_2R species isoforms with guanidines, 2) that a single amino acid in transmembrane domain 7 critically determines guanidine potency, and 3) that an interaction between transmembrane domains 1 and 7 is important for guanidine efficacy.

HIS (**1**) is a biogenic amine (Fig. 1) that functions as a neurotransmitter and autacoid (Hill et al., 1997). HIS exerts its effects through at least four receptor subtypes, designated H_1, H_2, H_3, and H_4, respectively (Hill et al., 1997; Hough, 2001). HIS receptors belong to the superfamily of GPCRs that possess seven transmembrane domains, three extracellular and three intracellular loops. The H_2R couples to G_s-proteins to activate adenylyl cyclase. Numerous H_2R agonists and antagonists have been developed; the guinea pig atrium has been the standard model for ligand design for decades (Ganellin, 1982; Hill et al., 1997). Figure 1 shows the structures of prototypical H_2R agonists and antagonists. Among agonists, DIM (**2**), AMT (**3**), and BET (**4**) are similar to HIS (**1**). BET is a nonselective H_2R partial agonist (Ganellin, 1982; Burde et al., 1989) and is therefore an interesting experimental tool. Compared with compounds **1** to **4**, the guanidines **5** to **13** are long-chained and more bulky. IMP (**5**), ARP (**8**), and several ARP analogs are much more potent in the guinea pig atrium than HIS (Durant et al., 1978;

This work was supported by a New Faculty Award of The University of Kansas (R.S.), the National Institutes of Health COBRE award 1-P20-RR15563, matching support from the State of Kansas and the University of Kansas (R.S.), grants of the Fonds der Chemischen Industrie (A.B.), and the Deutscher Akademischer Austauschdienst within the international network "Medicinal Chemistry" (A.B.). M.T.K. and T.B. contributed equally to this work.

[1] Present address: Quintiles Inc., Kansas City, Missouri.

ABBREVIATIONS: HIS, histamine; AMT, amthamine; DIM, dimaprit; BET, betahistine; GPCR, G-protein-coupled receptor; H_xR, histamine H_x-receptor, where *x* is 1, 2, 3, or 4; IMP, impromidine; ARP, arpromidine; CIM, cimetidine; RAN, ranitidine; FAM, famotidine; TIO, tiotidine; ZOL, zolantidine; APT, aminopotentidine; h, human; gp, guinea pig; G_s-proteins, family of G-proteins that mediates adenylyl cyclase activation; $G_{s\alpha S}$, short splice variant of the G_s-protein $G_{s\alpha}$; $G_{s\alpha L}$, long splice variant of the G_s-protein $G_{s\alpha}$; β_2AR, β_2-adrenoceptor; β_2AR-$G_{s\alpha L}$, fusion protein containing the β_2AR and the long splice variant of $G_{s\alpha}$; DHA, dihydroalprenolol; PCR, polymerase chain reaction; bp, base pair(s); 3D QSAR, three-dimensional quantitative structure-activity relationship; gpH_2R-$G_{s\alpha S}$, fusion protein of the guinea pig histamine H_2-receptor and the short splice variant of $G_{s\alpha}$; hH_2R-A271D-$G_{s\alpha S}$, fusion protein of the human histamine H_2-receptor bearing an Ala→Asp mutation at position 271 and the short splice variant of $G_{s\alpha}$; hH_2R-$G_{s\alpha S}$, fusion protein of the human histamine H_2-receptor and the short splice variant of $G_{s\alpha}$; NhCgpH_2R-$G_{s\alpha S}$, fusion protein consisting of the N-terminal half of the human histamine H_2-receptor, the C-terminal half of the guinea pig histamine H_2-receptor, and the short splice variant of $G_{s\alpha}$; NgpChH_2R-$G_{s\alpha S}$, fusion protein consisting of the N-terminal half of the guinea pig histamine H_2-receptor, the C-terminal half of the human histamine H_2-receptor, and the short splice variant of $G_{s\alpha}$; TM, transmembrane domain of a G-protein-coupled receptor; PAGE, polyacrylamide gel electrophoresis.

MOLECULAR PHARMACOLOGY
aspet
Downloaded from molpharm.aspetjournals.org by guest on December 1, 2012

MOL PHARM

MOLECULAR PHARMACOLOGY

Buschauer, 1989). H_2R antagonists are divided into five chemical classes: imidazoles such as CIM (**14**), furans such as RAN (**15**), thiazoles such as FAM (**16**), and TIO (**17**), piperidinomethylphenoxy derivatives such as ZOL (**18**), and (benzamidoalkyl)cyanoguanidines such as APT (**19**) (Hill et al., 1997). H_2R antagonists are of great importance for the treatment of gastroduodenal ulcer disease (Hill et al., 1997). H_2R agonists may be useful as positive inotropic drugs for the treatment of heart failure (Felix et al., 1995), as differentiation-inducing agents in acute myelogenous leukemia (Seifert et al., 1992), and as anti-inflammatory drugs (Burde et al., 1990).

Guanidine-type compounds are less potent and/or efficient agonists at the H_2R of human neutrophils than at the H_2R of the guinea pig atrium (Burde et al., 1989, 1990; Buschauer, 1989). Additionally, several GPCR species isoforms, including the H_3R, differ from each other in their pharmacological properties as assessed by the analysis of recombinant GPCRs (Kopin et al., 2000; Ligneau et al., 2000; Lovenberg et al., 2000). There are relatively few amino acid differences between hH_2R and gpH_2R (Gantz et al., 1991; Traiffort et al., 1995) (Fig. 2), particularly in the established ligand-binding domains TM3 and TM5, but even a single amino acid exchange between GPCR species isoforms can strongly affect their pharmacological properties (Kopin et al., 2000; Ligneau et al., 2000). Based on these findings, the hypothesis arose that the H_2R exhibits species-specific pharmacological properties as well.

To test our hypothesis, we constructed fusion proteins of the hH_2R and gpH_2R, respectively, and $G_{s\alpha S}$ and expressed the fusion proteins in Sf9 cell membranes. GPCR-G_α fusion proteins ensure a defined 1:1 stoichiometry of the signaling partners and efficient coupling (Seifert et al., 1999; Milligan, 2000). The measurement of GTP hydrolysis in GPCR-G_α fusion proteins is presumably the most precise method currently available for the analysis of ligand potencies and efficacies, because the GTPase assay is a steady-state method, is extremely sensitive in GPCR-$G_{s\alpha}$ fusion proteins, assesses GPCR/G-protein coupling directly at the G-protein level, and is independent of the expression level of the components (Seifert et al., 1999; Milligan, 2000). Finally, the analysis of H_2R species isoforms in the same host cell membrane annihilates the impact of pharmacokinetic differences between different test systems. Here, we report that hH_2R and gpH_2R exhibit distinct pharmacological properties, particularly with respect to interaction with guanidines.

Experimental Procedures

Materials. The cDNA for the hH_2R was kindly provided by Dr. I. Gantz (University of Michigan Medical School and Ann Arbor VA Medical Center, Ann Arbor, MI) (Gantz et al., 1991). The cDNA for the gpH_2R was kindly provided by Drs. E. Traiffort and J.-C. Schwartz (Department of Neurobiology and Pharmacology, Center Paul Broca, Institut National de la Santé et de la Recherche Médicale, Paris, France) (Traiffort et al., 1995). The generation of the baculovirus encoding β_2AR-$G_{s\alpha L}$ had been described previously (Seifert et al., 1998a). APT was synthesized as described previously (Hirschfeld et al., 1992). IMP was prepared as described previously (Durant et al., 1978). Guanidines **6** to **11** were synthesized as described previously (Buschauer, 1989). Guanidines **12** and **13** (Schalkhausser, 1998) were prepared by analogy to the procedures described for guanidines **6** to **11** (Buschauer, 1989). The structures of the synthesized compounds were confirmed by analysis (C, H, N), ^{1}H NMR, and mass spectroscopy spectra. Purity of compounds was >98% as determined by high-performance liquid chromatography or capillary electrophoresis (Schuster et al., 1997). The anti-FLAG Ig (M1 monoclonal antibody) was from Sigma (St. Louis, MO). The

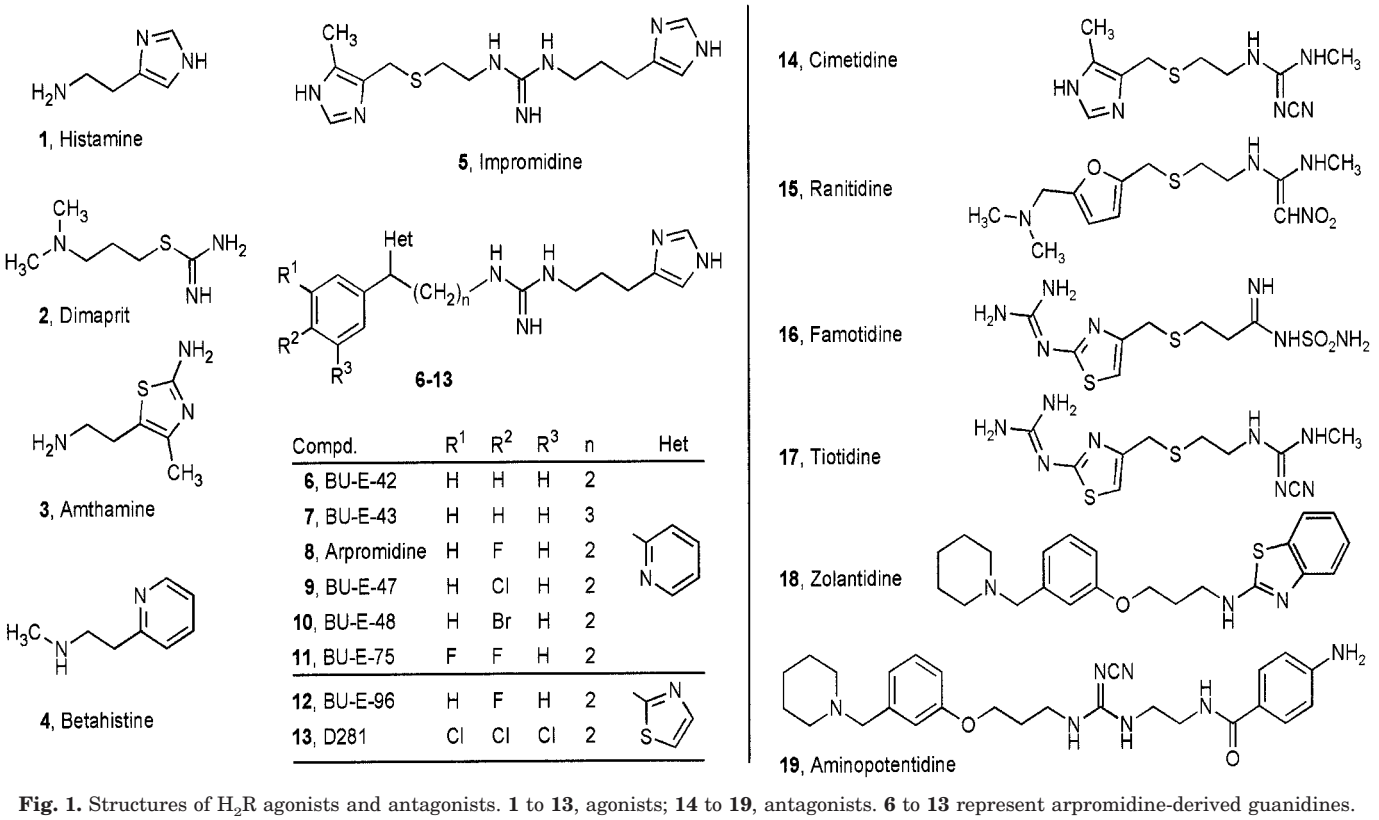

Compd.	R^1	R^2	R^3	n	Het
6, BU-E-42	H	H	H	2	
7, BU-E-43	H	H	H	3	
8, Arpromidine	H	F	H	2	
9, BU-E-47	H	Cl	H	2	
10, BU-E-48	H	Br	H	2	
11, BU-E-75	F	F	H	2	
12, BU-E-96	H	F	H	2	
13, D281	Cl	Cl	Cl	2	

Fig. 1. Structures of H_2R agonists and antagonists. **1** to **13**, agonists; **14** to **19**, antagonists. **6** to **13** represent arpromidine-derived guanidines.

Downloaded from molpharm.aspetjournals.org by guest on December 1, 2012

MOL PHARM

MOLECULAR PHARMACOLOGY

anti-$G_{s\alpha}$ Ig (C-terminal) was from Calbiochem (La Jolla, CA). [γ-^{32}P]GTP (6000 Ci/mmol), [^{35}S]GTPγS (1100 Ci/mmol), [^{3}H]DHA (85–90 Ci/mmol), and [^{3}H]TIO (90 Ci/mmol) were from PerkinElmer Life Sciences (Boston, MA). All unlabeled nucleotides were from Roche (Indianapolis, IN). HIS, BET, CIM, RAN, and FAM were from Sigma. AMT, TIO, and ZOL were from Tocris Cookson (Ballwin, MO). DIM was from RBI (Natick, MA). All restriction enzymes and T4 DNA ligase were from New England Biolabs (Beverly, MA). Cloned *Pfu* DNA polymerase was from Stratagene (La Jolla, CA).

Construction of FLAG Epitope- and Hexahistidine-Tagged cDNA for hH_2R-$G_{s\alpha S}$. A DNA sequence encoding the cleavable signal peptide from influenza hemagglutinin (S) followed by the FLAG epitope (F), which is recognized by the M1 antibody, was placed 5′ of the start codon of the hH_2R to enhance GPCR expression and allow immunological detection. We also added a hexahistidine tag to the C terminus of hH_2R to allow future purification and to provide additional protection against proteolysis (Seifert et al., 1998a). The GPCR modifications were generated by sequential overlap-extension PCRs. In PCR 1A, the DNA sequence of the N-terminal portion of the hH_2R was amplified using CMVneo-hH_2R as template. The sense primer annealed with the first 18 bp of the 5′-end of the hH_2R and included the last 18 bp of the SF in its 5′-extension. The antisense primer encoded the sequence GAGCTGTTGATATCCGGTGCGGAAGTCTCTG to generate a silent mutation yielding a new *Eco*RV site. In PCR 1B, the DNA sequence of the C-terminal portion of the hH_2R was amplified using CMVneo-hH_2R as template. The sense primer encoded the sequence TTCCGCACCGGATATCAACAGCTCTTCTGCTGC to generate the new *Eco*RV site. The antisense primer encoded the five C-terminal amino acids of the hH_2R, a hexahistidine tag, the stop codon and an *Xba*I site. In PCR 2, the products of PCRs 1A and 1B annealed in the region encoding the newly created *Eco*RV site. In PCR 2, the sense primer of PCR 1A and the antisense primer of PCR 1B were used. In this way, a fragment encoding the signal sequence, the FLAG epitope, hH_2R cDNA with a new *Eco*RV site and a hexahistidine tag followed by an *Xba*I site was obtained. This fragment was digested with *Nco*I and *Xba*I and cloned into pGEM-3Z-SF-human formyl peptide receptor-6His digested with *Nco*I and *Xba*I. In PCR 3A, the C-terminal portion of the H_2R was amplified using pGEM-3Z-SF-hH_2R as template, a sense primer annealing 5′ of the newly created *Eco*RV site and an antisense primer annealing with the hexahistidine tag. In PCR 3B, the sequence of $G_{s\alpha S}$ was amplified, using pGEM-3Z-SF-β_2AR-$G_{s\alpha S}$ as template, a sense primer annealing with the hexahistidine tag and an antisense primer annealing with the 5 C-terminal amino acids of $G_{s\alpha}$, the stop codon, and an *Xba*I site. In PCR 4, the products of PCRs 3A and 3B annealed in the hexahistidine region, and the sense primer of PCR 3A and the antisense primer of PCR 3B were used. In this way, a fragment encoding the C-terminal portion of the hH_2R, a hexahistidine tag, $G_{s\alpha S}$, a stop codon and an *Xba*I site was created. This fragment was digested with *Eco*RV and *Xba*I and cloned into pGEM-3Z-SFhH_2R digested with *Eco*RV and *Xba*I. In this way, the full-length cDNA for hH_2R-$G_{s\alpha S}$ was created. pGEM-3Z-SF-hH_2R-$G_{s\alpha S}$ was digested with *Nco*I and *Xba*I to recover the fusion protein cDNA and cloned into the baculovirus transfer vector pVL 1392-SF-β_2AR-$G_{i\alpha 2}$ digested with *Nco*I and *Xba*I. PCR-generated DNA sequences were confirmed by extensive restriction enzyme analysis and enzymatic sequencing.

Construction of FLAG Epitope- and Hexahistidine-Tagged cDNA for gpH_2R-$G_{s\alpha S}$. The strategy for creation of gpH_2R-$G_{s\alpha S}$ cDNA was analogous to the strategy for creation of hH_2R-$G_{s\alpha S}$ cDNA. In PCR 1A, the DNA sequence of the N-terminal portion of gpH_2R was amplified using pGEM4Z-gpH_2R as template. The sense primer annealed with the first 20 bp of the 5′-end of the gpH_2R and included the last 8 bp of the SF in its 5′-extension. The antisense primer encoded the sequence CTCATGGGAGTTGTGGCTAGCGAGCCTGCAGCAGAAGAGC to create a silent mutation yielding a new *Nhe*I site. In PCR 1B, the sequence of the C-terminal portion of gpH_2R was amplified using pGEM4Z-gpH_2R as template. The sense primer encoded the sequence GCTCTTCTGCTGCAGGCTCGCTAGCCACAACTCCCATGAG to create the new *Nhe*I site. The antisense primer encoded the five C-terminal amino acids of the gpH_2R, a hexahistidine tag, the stop codon, and an *Xba*I site. In PCR 2, the products of PCRs 1A and 1B annealed in the region encoding the newly created *Nhe*I site. In PCR 2, the sense primer of PCR 1A and the antisense primer of PCR 1B were used. In this way, a fragment encoding the signal sequence, the FLAG epitope, gpH_2R cDNA with a new *Nhe*I site, and a hexahistidine tag followed by an *Xba*I site was obtained. This fragment was digested with *Nco*I and *Xba*I and cloned into pGEM-3Z-SF-human formyl peptide receptor-6His digested with *Nco*I and *Xba*I. In PCR 3A, the C-terminal portion of the gpH_2R was amplified using pGEM-3Z-SF-gpH_2R as template, a sense primer annealing 5′ of the newly created *Nhe*I site, and an antisense primer annealing with the hexahistidine tag. In PCR 3B, the sequence of $G_{s\alpha S}$ was amplified, using pGEM-3Z-SF-β_2AR-$G_{s\alpha S}$ as tem-

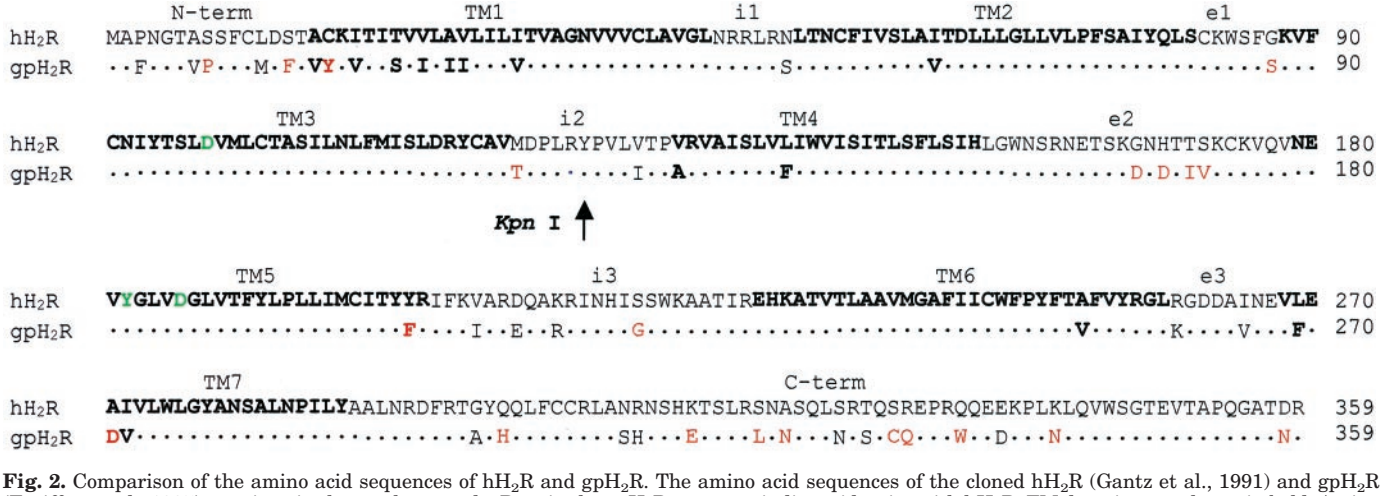

Fig. 2. Comparison of the amino acid sequences of hH_2R and gpH_2R. The amino acid sequences of the cloned hH_2R (Gantz et al., 1991) and gpH_2R (Traiffort et al., 1995) are given in the one-letter code. Dots in the gpH_2R sequence indicate identity with hH_2R. TM domains are shown in bold. Amino acids shown in green in TM3 and TM5 represent the interaction sites of HIS with the H_2R (Gantz et al., 1992; Nederkoorn et al., 1996). Amino acids shown in black in the gpH_2R sequence represent conservative exchanges. Amino acids shown in red in the gpH_2R sequence represent nonconservative exchanges. The arrow indicates the cleavage site of *Kpn*I, present in the cDNA of both gpH_2R and hH_2R. The *Kpn*I site allowed us to construct reciprocal hH_2R/gpH_2R chimeras (see Fig. 10). *N*-term, extracellular N-terminal domain of H_2Rs; C-term, intracellular C-terminal domain of H_2Rs.; i1, i2, and i3; 1st, 2nd, and 3rd intracellular loop, respectively; e1, e2, and e3, 1st, 2nd, and 3rd extracellular loop, respectively; TM1–7, transmembrane domains 1–7.

Downloaded from molpharm.aspetjournals.org by guest on December 1, 2012

MOL PHARM

MOLECULAR PHARMACOLOGY

plate, a sense primer annealing with the hexahistidine tag, and an antisense primer annealing with the 5 C-terminal amino acids of $G_{s\alpha}$, the stop codon, and an *Xba*I site. In PCR 4, the products of PCRs 3A and 3B annealed in the hexahistidine region, and the sense primer of PCR 3A and the antisense primer of PCR 3B were used. In this way, a fragment encoding the C-terminal portion of the gpH_2R, a hexahistidine tag, $G_{s\alpha S}$, a stop codon, and an *Xba*I site was created. This fragment was digested with *Nhe*I and *Xba*I and cloned into pGEM-3Z-SFgpH_2R digested with *Nhe*I and *Xba*I. In this way, the full-length cDNA for gpH_2R-$G_{s\alpha S}$ was created. pGEM-3Z-SF-hH_2R-$G_{s\alpha S}$ was digested with *Nco*I and *Xba*I to recover the fusion protein cDNA and cloned into the baculovirus transfer vector pVL 1392-SF-β_2AR-$G_{i\alpha 2}$ digested with *Nco*I and *Xba*I. PCR-generated DNA sequences were confirmed by extensive restriction enzyme analysis and enzymatic sequencing.

Construction of the cDNA for hH_2R-A271D-$G_{s\alpha S}$. The Ala-271 → Asp-271 exchange in hH_2R was generated by sequential overlap-extension PCRs. In PCR 1A, the DNA sequence of the N-terminal portion of hH_2R was amplified using pGEM-3Z-SF-hH_2R-$G_{s\alpha S}$ as a template. The sense primer annealed with the first 18 bp of the 5′ end of hH_2R and included the last 18 bp of the SF in its 5′ extension. The antisense primer encoded the sequence CAGAACGATATCTCTTCTAACACCTCATTGATGGCATC to generate the Ala-271 → Asp-271 exchange and a new *Eco*RV site at the position of the mutated amino acid. In PCR 1B, the DNA sequence of the C-terminal portion of the hH_2R and the entire sequence of $G_{s\alpha}$s was amplified using pGEM-3Z-SF-hH_2R-$G_{s\alpha S}$ as a template. The sense primer encoded the sequence GTTAGAAGATATCGTTCTGTGGCTGGGCTATGCCAAC to generate the Ala-271 → Asp-271 exchange and a new *Eco*RV site at the position of the mutated amino acid. The antisense primer encoded the five C-terminal amino acids of $G_{s\alpha}$, the stop codon and an *Xba*I site. In PCR 2, the products of PCR 1A and 1B annealed in the region encoding the newly created Ala-271 → Asp-271 exchange and the *Eco*RV site. In the PCR 2, the sense primer of PCR 1A and the antisense primer of PCR 1B were used. In this way, a fragment encoding the entire hH_2R-A271D-$G_{s\alpha S}$ fusion protein was created. This fragment was digested with *Eco*RI and *Nco*I and cloned into pGEM-3Z-SF-hH_2R-$G_{s\alpha S}$ digested with *Eco*RI and *Nco*I. pGEM-3Z-SF-hH_2R-A271D-$G_{s\alpha S}$ was digested with *Sac*I and *Eco*N I and cloned into the baculovirus transfer vector pVL 1392-SF-hH_2R-$G_{s\alpha S}$ digested with *Sac*I and *Eco*N I. PCR-generated DNA sequences were confirmed by extensive restriction enzyme analysis and enzymatic sequencing.

Construction of the cDNAs for NgpChH_2R-$G_{s\alpha S}$ and NhCgpH_2R-$G_{s\alpha S}$. For construction of hH_2R/gpH_2R chimeras, we took advantage of the *Kpn*I site present at the same position of the cDNAs of both receptors. *Kpn*I cleaves hH_2R- and gpH_2R cDNA in the center of the second intracellular loop (Fig. 2). pGEM-3Z-SF-hH_2R-$G_{s\alpha S}$ and pGEM-3Z-SF-gpH_2R-$G_{s\alpha S}$ were digested with *Kpn*I and *Xba*I so that the C-terminal halves of H_2Rs and the fused $G_{s\alpha S}$ were cut out. The fragments obtained were reciprocally cloned back into pGEM-3Z-SF-hH_2R-$G_{s\alpha S}$ and pGEM-3Z-SF-gpH_2R-$G_{s\alpha S}$. As a result of this exchange, we created pGEM-3Z-SF-NgpChH_2R-$G_{s\alpha S}$ and pGEM-3Z-SF-NhCgpH_2R-$G_{s\alpha S}$. These plasmids were digested with *Nco*I and *Xba*I and cloned into the baculovirus transfer vector pVL 1392-SF-gpH_2R-$G_{s\alpha S}$ digested with *Nco*I and *Xba*I. The chimeric H_2R-$G_{s\alpha S}$ DNA sequences were confirmed by extensive restriction enzyme analysis.

Generation of Recombinant Baculoviruses, Cell Culture and Membrane Preparation. Recombinant baculoviruses encoding the H_2R-$G_{s\alpha}$ fusion proteins were generated in Sf9 cells using the BaculoGOLD transfection kit (BD PharMingen, San Diego, CA) according to the manufacturer's instructions. After initial transfection, high-titer virus stocks were generated by two sequential virus amplifications. Sf9 cells were cultured in 250-ml disposable Erlenmeyer flasks at 28°C under rotation at 125 rpm in SF 900 II medium (Invitrogen, Carlsbad, CA) supplemented with 5% (v/v) fetal calf serum (BioWhittaker, Walkersville, MD) and 0.1 mg/ml gentamicin (BioWhittaker). Cells were maintained at a density of 0.5 to 6.0 × 10^6 cells/ml. For infection, cells were sedimented by centrifugation and suspended in fresh medium. Cells were seeded at 3.0 × 10^6 cells/ml and infected with a 1:100 dilution of high-titer baculovirus stocks encoding H_2R-$G_{s\alpha S}$ fusion proteins. Cells were cultured for 48 h before membrane preparation. Sf9 membranes were prepared as described previously (Seifert et al., 1998a), using 1 mM EDTA, 0.2 mM phenylmethylsulfonyl fluoride, 10 μg/ml benzamidine, and 10 μg/ml leupeptin as protease inhibitors. Membranes were suspended in binding buffer (12.5 mM $MgCl_2$, 1 mM EDTA and 75 mM Tris/HCl, pH 7.4) and stored at −80°C until use.

Receptor Ligand Binding Assays. Membranes were thawed and sedimented by a 15-min centrifugation at 4°C and 15,000*g* to remove residual endogenous guanine nucleotides as much as possible. Membranes were resuspended in binding buffer (12.5 mM $MgCl_2$, 1 mM EDTA and 75 mM Tris/HCl, pH 7.4). In [^{3}H]TIO binding assays, each tube (total volume, 250 μl) contained 200 to 250 μg of protein. Nonspecific binding was determined in the presence of [^{3}H]TIO at various concentrations plus 100 μM unlabeled TIO. Incubations were conducted for 90 min at 25°C and shaking at 250 rpm. In saturation binding experiments, tubes contained 1 to 20 nM [^{3}H]TIO plus unlabeled TIO to obtain final ligand concentrations of up to 300 nM. Competition binding experiments were carried out in the presence of 10 nM [^{3}H]TIO and unlabeled ligands at various concentrations without or with GTPγS (10 μM). Bound [^{3}H]TIO was separated from free [^{3}H]TIO by filtration through GF/C filters, followed by three washes with 2 ml of binding buffer (4°C). Filter-bound radioactivity was determined by liquid scintillation counting. The experimental conditions chosen ensured that not more than 5% of the total amount of [^{3}H]TIO added to binding tubes was bound to filters. The expression level of β_2AR-$G_{s\alpha L}$ was determined with 10 nM [^{3}H]DHA as radioligand as described previously (Seifert et al., 1998a).

[^{35}S]GTPγS Binding Assay. Membranes were thawed, sedimented, and suspended as for receptor ligand binding assays. Reaction mixtures (total volume, 500 μl) contained Sf9 membranes expressing H_2R-$G_{s\alpha}$ fusion proteins (15 μg of protein/tube) in binding buffer supplemented with 0.05% (w/v) bovine serum albumin, 1 μM GDP, and 1 nM [^{35}S]GTPγS plus 9 nM unlabeled GTPγS. Reaction mixtures additionally contained distilled water (basal) and HIS at a saturating concentration (100 μM). Incubations were conducted for 90 min at 25°C and shaking at 250 rpm. Bound [^{35}S]GTPγS was separated from free [^{35}S]GTPγS by filtration through GF/C filters, followed by three washes with 2 ml of binding buffer (4°C). Filter-bound radioactivity was determined by liquid scintillation counting. The experimental conditions chosen ensured that no more than 10% of the total amount of [^{35}S]GTPγS added was bound to filters.

Steady-State GTPase Activity Assay. Membranes were thawed, sedimented, and resuspended in 10 mM Tris/HCl, pH 7.4. Assay tubes contained Sf9 membranes expressing H_2R-$G_{s\alpha}$ fusion proteins (10 μg of protein/tube), 1.0 mM $MgCl_2$, 0.1 mM EDTA, 0.1 mM ATP, 100 nM GTP, 1 mM adenylyl imidodiphosphate, 5 mM creatine phosphate, 40 μg of creatine kinase, and 0.2% (w/v) bovine serum albumin in 50 mM Tris/HCl, pH 7.4, and H_2R ligands at various concentrations. Reaction mixtures (80 μl) were incubated for 3 min at 25°C before the addition of 20 μl of [γ-^{32}P]GTP (0.2–0.5 μCi/tube). All stock and work dilutions of [γ-^{32}P]GTP were prepared in 20 mM Tris/HCl, pH 7.4. Reactions were conducted for 20 min at 25°C. Preliminary studies under basal conditions and with HIS, IMP, and ARP showed that under these conditions, GTP hydrolysis was linear. Reactions were terminated by the addition of 900 μl of slurry consisting of 5% (w/v) activated charcoal and 50 mM NaH_2PO_4, pH 2.0. Charcoal absorbs nucleotides but not P_i. Charcoal-quenched reaction mixtures were centrifuged for 15 min at room temperature at 15,000*g*. Seven hundred microliters of the supernatant fluid of reaction mixtures were removed, and $^{32}P_i$ was determined by liquid scintillation counting. Enzyme activities were corrected for spontaneous degradation of [γ-^{32}P]GTP. Spontaneous

Downloaded from molpharm.aspetjournals.org by guest on December 1, 2012

MOL PHARM

MOLECULAR PHARMACOLOGY

[γ-^{32}P]GTP degradation was determined in tubes containing all of the above described components plus a very high concentration of unlabeled GTP (1 mM) that, by competition with [γ-^{32}P]GTP, prevents [γ-^{32}P]GTP hydrolysis by enzymatic activities present in Sf9 membranes. Spontaneous [γ-^{32}P]GTP degradation was <1% of the total amount of radioactivity added using 20 mM Tris/HCl, pH 7.4, as solvent for [γ-^{32}P]GTP. The experimental conditions chosen ensured that not more than 10% of the total amount of [γ-^{32}P]GTP added was converted to $^{32}P_i$.

SDS-PAGE and Immunoblot Analysis. Membrane proteins were separated on SDS polyacrylamide gels containing 8% (w/v) acrylamide. Proteins were then transferred onto Immobilon-P transfer membranes (Millipore, Bedford, MA). Membranes were reacted with M1 antibody or anti-$G_{s\alpha}$ Ig (1:1000 each). Immunoreactive bands were visualized by sheep anti-mouse IgG (M1 antibody) and donkey anti-rabbit IgG (anti-$G_{s\alpha}$ Ig), respectively, coupled to peroxidase, using *o*-dianisidine and H_2O_2 as substrates.

Molecular Modeling. Models of the seven TM helices were taken from the PDB bovine rhodopsin file 1f88 (Palczewski et al., 2000). The starting structure of gpH_2R TM domains was constructed from a multiple sequence-alignment of bovine rhodopsin with hβ_2AR (Palczewski et al., 2000), gpH_1R, hH_2R, and gpH_2R (Gantz et al., 1991; Traiffort et al., 1995; Hill et al., 1997). The resulting TM helices in hH_2R and gpH_2R are highlighted in bold (Fig. 2). First, the model was roughly minimized by the steepest descent method to remove bad contacts due to the mutated residues. In the first 100 steps, the backbone was fixed. Energy calculations were based on the Kollman all-atom force field (Kollman charges, distant dependent dielectricity constant of 4). Then IMP (**5**) and ARP (**8**) were manually docked into the model in a conformation suggested to be active from 3D QSAR results (Dove and Buschauer, 1998, 1999). The selection of amino acids interacting with the imidazolylpropylguanidine moiety based on studies with hH_2R (Gantz et al., 1992), hβ_2AR (Wieland et al., 1996; Isogaya et al., 1999), and hH_1R (Wieland et al., 1999) mutants. The docking with respect to TM 6 and 7 was only roughly suggested by seeking a pocket near the "hot" region around Asp-271 that may accommodate the imidazole and the pyridine moiety of IMP and ARP, respectively. Kollman all-atom types were assigned to IMP and ARP by analogy, including definition of the new atom type F (fluorine). Missing parameters (e.g., for bonds CA—NB, CC—CC, F—CA, and a number of bond angles) were derived from similar types or from the Tripos force field. As hydrogen bonding parameters for F-H3, the respective values for O and N were assigned. Both ligands were provided with Gasteiger-Hueckel charges. The complexes were fully minimized (distant dependent dielectricity constant of 1) without constraints by the Powell method down to an RMS gradient of less than 0.05. All calculations were performed with SYBYL 6.7 (Tripos, St. Louis, MO) on an SGI Octane workstation (SGI, Mountain View, CA)

Miscellaneous. Protein concentrations were determined using the DC protein assay kit (Bio-Rad, Hercules, CA). All analyses of experimental data were performed with the Prism III program (GraphPad Software, San Diego, CA).

Results and Discussion

Immunological Detection of hH_2R-$G_{s\alpha S}$ and gpH_2R-$G_{s\alpha S}$ in Sf9 Cell Membranes. Monomeric nonfused H_2R expressed in Sf9 cells migrates as ~33-kDa band in SDS-PAGE (Fukushima et al., 1997), and the apparent molecular mass of $G_{s\alpha S}$ is ~45 kDa. Thus, the molecular mass of H_2R-$G_{s\alpha S}$ fusion proteins was expected to be ~78 kDa. In fact, the anti-FLAG Ig detected a ~78-kDa band in immunoblots (Fig. 3). The intensities of immunologically detected bands in membranes expressing hH_2R-$G_{s\alpha S}$ and gpH_2R-$G_{s\alpha S}$ were similar to the band intensities in membranes expressing β_2AR-$G_{s\alpha L}$ fusion protein at 7.0 pmol/mg as determined by [^{3}H]DHA saturation binding. The ~44-kDa band in membranes expressing β_2AR-$G_{s\alpha L}$ represents a degradation product of the fusion protein that was generated as the result of incidental freeze/thaw cycles. The membranes expressing H_2R-$G_{s\alpha S}$ did not undergo such cycles, and accordingly, we did not observe degradation products. In membranes expressing hH_2R-$G_{s\alpha S}$ and, to a much lesser extent, in membranes expressing gpH_2R-$G_{s\alpha S}$, we also observed ~160-kDa bands. The H_2R is known to form homodimers (Fukushima et al., 1997), and thus the ~160-kDa bands most probably represent H_2R-$G_{s\alpha S}$ fusion protein homodimers.

[^{3}H]TIO- and [^{35}S]GTPγS Saturation Binding to hH_2R-$G_{s\alpha S}$ and gpH_2R-$G_{s\alpha S}$ Expressed in Sf9 Cell Membranes. Native gpH_2R binds [^{3}H]TIO with a K_d value of ~17 nM (Gajtkowski et al., 1983). However, the use of [^{3}H]TIO in native organs is severely limited by the fact that nonspecific binding with saturating [^{3}H]TIO concentrations amounts to ~85 to 90% of total [^{3}H]TIO binding. In Sf9 membranes, only ~55 to 65% nonspecific [^{3}H]TIO binding occurred with saturating radioligand concentrations. Therefore, a more precise

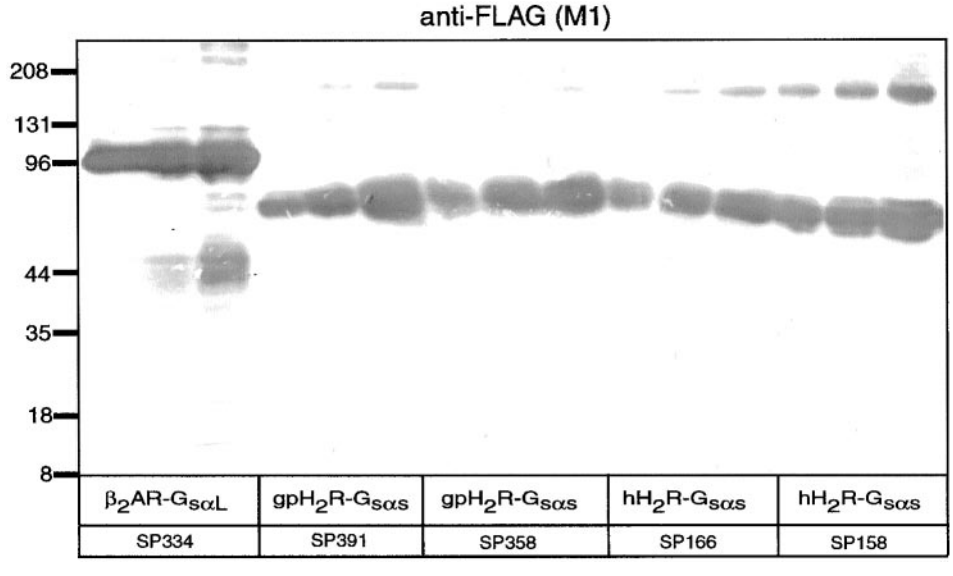

Fig. 3. Analysis of the expression of H_2R-$G_{s\alpha S}$ fusion proteins in Sf9 cell membranes. Various Sf9 cell membrane preparations (SP followed by number) expressing β_2AR-$G_{s\alpha L}$ (7.0 pmol/mg as assessed by [^{3}H]DHA saturation binding) and H_2R-$G_{s\alpha}$ fusion proteins were separated by SDS-PAGE using a gel that contained 8% (w/v) acrylamide. Fusion proteins were probed with the anti-FLAG Ig (M1 antibody). Each membrane preparation was analyzed in three different amounts (25, 50, and 100 μg of protein, respectively, from left to right). Numbers on the left of the immunoblot indicate molecular masses of marker proteins. Shown is the horseradish peroxidase-reacted Immobilon P membrane of a representative gel. Similar results were obtained with four other membrane preparations of hH_2R-$G_{s\alpha S}$ and gpH_2R-$G_{s\alpha S}$ each.

Downloaded from molpharm.aspetjournals.org by guest on December 1, 2012

MOL PHARM
MOLECULAR PHARMACOLOGY
aspet

determination of the kinetics of specific [^{3}H]TIO binding was possible (Fig. 4). H_2R-$G_{s\alpha S}$ fusion proteins expressed in Sf9 membranes bound [^{3}H]TIO according to monophasic saturation curves: hH_2R-$G_{s\alpha S}$ with a K_d value of 32.0 ± 4.6 nM and a B_{max} value of 0.43 ± 0.02 pmol/mg (SP166); gpH_2R-$G_{s\alpha S}$ with a K_d value of 34.4 ± 8.4 nM and a B_{max} value of 0.72 ± 0.02 pmol/mg (SP391). Although the K_d values for [^{3}H]TIO fit well to the K_B values for TIO in the GTPase competition studies with HIS (Table 1), we would have expected B_{max} values of ~5 to 7 pmol/mg for H_2R-$G_{s\alpha S}$ fusion proteins.

There are two possible explanations for the low B_{max} values of [^{3}H]TIO binding to H_2R-$G_{s\alpha S}$ fusion proteins. [^{3}H]TIO could either bind to only a fraction of the functionally active fusion protein molecules or the majority of the expressed molecules could be inactive. To discriminate between these alternatives, we took advantage of the fact that in GPCR-G_α fusion proteins, 1 mol of protein binds ~1 mol of [^{35}S]GTPγS when fully activated (Wenzel-Seifert and Seifert, 2000; Liu et al., 2001). The B_{max} value of HIS-stimulated [^{35}S]GTPγS binding was 5.2 ± 0.6 pmol/mg for hH_2R-$G_{s\alpha S}$ (SP166) and 8.7 ± 1.1 pmol/mg for gpH_2R-$G_{s\alpha S}$ (SP391). These values fit well to the immunological data (Fig. 3) and suggest that almost all of the expressed H_2R-$G_{s\alpha}$ molecules are functionally active. Accordingly, the majority of ligand-free H_2R-$G_{s\alpha}$ molecules exist in a conformation that does not bind [^{3}H]TIO. Future studies will have to determine whether H_2R-$G_{s\alpha}$ differentially binds [^{3}H]TIO and another H_2R radioligand, [^{125}I]iodoaminopotentidine (Hill et al., 1997).

Similar Antagonist Potencies at hH_2R-$G_{s\alpha S}$ and gpH_2R-$G_{s\alpha S}$ Expressed in Sf9 Cell Membranes and Evidence that RAN and APT Differentially Stabilize an Inactive Conformation in H_2R Species Isoforms. In GPCR-G_α fusion proteins, the GTPase assay is a highly sensitive method to determine ligand potencies and efficacies (Seifert et al., 1999; Milligan, 2000). GTP hydrolysis in Sf9 membranes expressing H_2R-$G_{s\alpha S}$ fusion proteins was stimulated with HIS at a submaximally effective concentration, and the HIS-stimulated GTP hydrolysis was inhibited by H_2R antagonists of various chemical classes. The K_B values

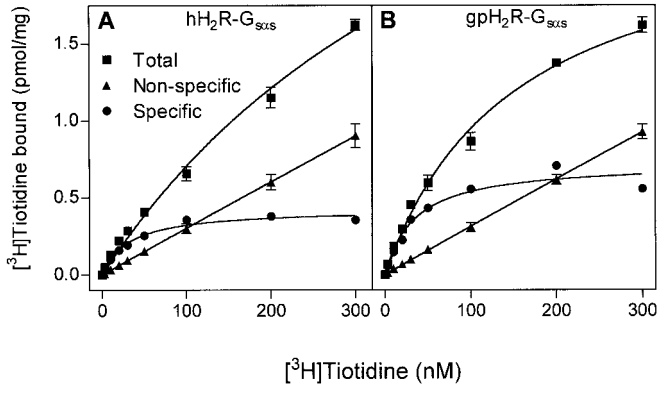

Fig. 4. [^{3}H]TIO saturation binding in Sf9 membranes expressing hH_2R-$G_{s\alpha S}$ and gpH_2R-$G_{s\alpha S}$. Membranes expressing hH_2R-$G_{s\alpha S}$ (A, SP166) or gpH_2R-$G_{s\alpha S}$ (B, SP391) were incubated in the presence of [^{3}H]TIO at the concentrations indicated on the abscissa as described under *Experimental Procedures*. Nonspecific binding is the [^{3}H]TIO binding not competed for by 100 μM unlabeled TIO. Specific binding is the difference between total [^{3}H]TIO binding and nonspecific [^{3}H]TIO binding for a given [^{3}H]TIO concentration. Data were analyzed by nonlinear regression and are the means ± S.D. of three experiments performed in duplicate. Similar results were obtained with four other membrane preparations of hH_2R-$G_{s\alpha S}$ and gpH_2R-$G_{s\alpha S}$ each.

for CIM (**14**), RAN (**15**), ZOL (**16**), TIO (**17**), FAM (**18**), and APT (**19**) did not vary by more than a factor of 2 between hH_2R-$G_{s\alpha S}$ and gpH_2R-$G_{s\alpha S}$ (Table 1). We correlated pK_B values of antagonists at hH_2R-$G_{s\alpha S}$ versus gpH_2R-$G_{s\alpha S}$. If the antagonist-affinities of hH_2R-$G_{s\alpha S}$ and gpH_2R-$G_{s\alpha S}$ were identical, we would expect a linear correlation with a slope of 1.00 that follows the dotted line in Fig. 5A. Indeed, we obtained a highly significant correlation with a slope of 0.98 close to the theoretical curve (Fig. 5A), indicating that the antagonist-binding properties of hH_2R-$G_{s\alpha S}$ and gpH_2R-$G_{s\alpha S}$ are very similar. This is an important finding, because for other GPCR species isoforms, including the H_3R, differences in antagonist-binding properties were observed (Kopin et al., 2000; Ligneau et al., 2000; Lovenberg et al., 2000).

Previous studies had shown that the hH_2R is constitutively active (i.e., H_2R antagonists decrease the activity of the agonist-free hH_2R) (Alewijnse et al., 1998). In fact, RAN (**15**) had a consistent inverse agonist effect at hH_2R-$G_{s\alpha S}$ (Table 1). APT (**19**), which had not been studied in this respect previously, was a much more efficient inverse agonist than RAN (**15**) at hH_2R-$G_{s\alpha S}$. At gpH_2R-$G_{s\alpha S}$, RAN showed the greatest inverse agonist effect among the antagonists studied, and the effect of RAN at gpH_2R-$G_{s\alpha S}$ was also significantly greater than at hH_2R-$G_{s\alpha S}$. Conversely, APT was considerably more efficient as an inverse agonist at hH_2R-$G_{s\alpha S}$ than at gpH_2R-$G_{s\alpha S}$. These data show that RAN and APT differentially stabilize an inactive conformation in hH_2R and gpH_2R. In support of the hypothesis that different H_2R antagonists stabilize unique conformations in H_2Rs from different species is the finding that at the rat H_2R, burimamide is a neutral antagonist, whereas at hH_2R, it is a partial agonist (Alewijnse et al., 1998).

The absolute inverse agonist activities of APT at hH_2R-$G_{s\alpha S}$ and of RAN at gpH_2R-$G_{s\alpha S}$, respectively, were similar, indicating that both GPCRs exhibit a similar degree of constitutive activity. In comparison, the rat H_2R is less constitutively active than hH_2R (Alewijnse et al., 1998). These data show that H_2R species isoforms differ from each other in their constitutive activity. Differences in constitutive activity among GPCR species isoforms are not restricted to the H_2R (Kopin et al., 2000). We also noted that, except for RAN (**15**) and APT (**19**), the inverse agonist effect of each individual antagonist was quite variable (Table 1). This variability does not reflect insensitivity of the GTPase assay. Rather, we assume that in our system, CIM (**14**), ZOL (**16**), TIO (**17**), and FAM (**18**) casually act as neutral antagonists or inverse agonists at H_2Rs, resulting in considerable data variability. Stochastic actions of weak inverse agonists were also reported for the β_2AR (Chidiac et al., 1996). Another factor that could have contributed to the relatively small inverse agonist effects of RAN and FAM at H_2R in this study relative to a previous study (Alewijnse et al., 1998) could be that we studied coupling of H_2Rs to $G_{s\alpha S}$ and not $G_{s\alpha L}$ (see *Experimental Procedures*). Specifically, it is known that $G_{s\alpha L}$ confers the properties of constitutive activity to the β_2AR; i.e., $G_{s\alpha L}$ increases inverse agonists effects, whereas $G_{s\alpha S}$ does not have these effects (Seifert et al., 1998b). Thus, it is possible that in the Chinese hamster ovary cells studied by Alewijnse et al. (1998), the H_2R was preferentially coupled to $G_{s\alpha L}$, thereby increasing inverse agonist effects.

Agonist Efficacies, Potencies and Affinities at hH_2R-$G_{s\alpha S}$ and gpH_2R-$G_{s\alpha S}$ Expressed in Sf9 Cell Mem-

Downloaded from molpharm.aspetjournals.org by guest on December 1, 2012

MOL PHARM

MOLECULAR PHARMACOLOGY

branes: Evidence that Guanidines Stabilize an Active Conformation in gpH_2R More Efficiently and Potently Than in hH_2R. We determined the efficacies and potencies of the small H_2R agonists **1** to **4** and of the larger H_2R agonists **5** to **13** in the GTPase assay (Table 2). The efficacies of HIS (**1**), DIM (**2**), AMT (**3**), and BET (**4**) were similar at hH_2R-$G_{s\alpha S}$ and gpH_2R-$G_{s\alpha S}$, respectively. In contrast, the efficacies of the guanidines **5** to **13** at hH_2R-$G_{s\alpha S}$ were all significantly lower than at gpH_2R-$G_{s\alpha S}$. The differences in efficacy were most prominent for BU-E-43 (**7**), BU-E-48 (**10**), and D281 (**13**). Specifically, elongation of the alkyl chain between the guanidino group and the phenyl ring (**6** → **7**) and introduction of a bulky Br atom (**6** → **10**) or of multiple Cl atoms into the phenyl ring (**12** → **13**) had pronounced negative effects on agonist efficacy at hH_2R-$G_{s\alpha S}$ but not at gpH_2R-$G_{s\alpha S}$. Accordingly, the slope of the correlation of the efficacies of agonists at hH_2R-$G_{s\alpha S}$ and gpH_2R-$G_{s\alpha S}$ was very shallow, and the theoretical curve assuming pharmacological identity of H_2R species isoforms was not approached within the data interval (Fig. 6A). Particularly informative is the comparison of the efficacies of BET (**4**) and guanidines **8** to **11**. At hH_2R-$G_{s\alpha S}$, these compounds possess efficacies of 0.73 to 0.87, but only guanidines have increased efficacies at gpH_2R-$G_{s\alpha S}$ (Table 2). Taken together, these results indicate that the hH_2R-$G_{s\alpha S}$ and gpH_2R-$G_{s\alpha S}$ conformations stabilized by one of the small agonists **1** to **4** similarly promote GDP/GTP exchange. In contrast, the guanidines **5** to **13** stabilize a hH_2R-$G_{s\alpha S}$ conformation considerably less efficient for GDP/GTP exchange than the corresponding gpH_2R-$G_{s\alpha S}$ conformation.

The potencies of small agonists (**1**–**4**) differed by not more than a factor of 2 between hH_2R-$G_{s\alpha S}$ and gpH_2R-$G_{s\alpha S}$ (Table 2). The correlation of the pD_2 values of compounds **1** to **4** at both H_2R-$G_{s\alpha S}$ was highly significant with a slope close to the theoretical curve assuming pharmacological identity of H_2R species isoforms (Fig. 5B). Except for BU-E-43 (**7**), the potencies of guanidines were all significantly lower at hH_2R-$G_{s\alpha S}$ than at gpH_2R-$G_{s\alpha S}$. Differences in potency between hH_2R-$G_{s\alpha S}$ and gpH_2R-$G_{s\alpha S}$ were particularly large for BU-E-75 (**11**) (6.6-fold), BU-E-42 (**6**) (6.0-fold), and IMP (**5**) (5.0-fold).

TABLE 1

Potencies and inverse agonist efficacies of antagonists at hH_2R-$G_{s\alpha S}$ and gpH_2R-$G_{s\alpha S}$ expressed in Sf9 cell membranes

K_B values for hH_2R-$G_{s\alpha S}$ and gpH_2R-$G_{s\alpha S}$ were determined in the GTPase assay. GTP hydrolysis was determined as described under *Experimental Procedures*. Reaction mixtures contained Sf9 membranes expressing fusion proteins, 1 μM HIS as agonist and antagonists at concentrations from 1 nM to 100 μM to generate saturated competition curves. Competition curves were analyzed by nonlinear regression. To determine the inverse agonist efficacies of antagonists (Inv. Ago. Eff.), the effects of antagonists at a fixed concentration (10 μM) on basal GTPase activity were assessed and referred to the stimulatory effect of 100 μM HIS (= 1.00). Typical basal GTPase activities ranged between ~1 and 2 pmol/mg/min, and typical GTPase activities stimulated by HIS (1 μM) ranged between ~2.5 and 5.0 pmol/mg/min. Data shown are the means of four to five experiments performed in duplicate. Numbers in parentheses represent the 95% confidence intervals. The relative potency (Rel. Pot.) of CIM was set at 100, and the potencies of other antagonists were measured against this value to facilitate comparison of antagonist potencies in the various systems. The effects of compounds at hH_2R-$G_{s\alpha S}$ were compared with the corresponding effects of compounds at gpH_2R-$G_{s\alpha S}$ using the t test.

Antagonist	hH_2R-$G_{s\alpha S}$			gpH_2R-$G_{s\alpha S}$		
	K_B	Rel. Pot.	Inv. Ago. Eff.	K_B	Rel. Pot.	Inv. Ago. Eff.
	nM			*nM*		
14 (CIM)	930 (460–1900)	100	−0.04 ± 0.04	1100 (400–2900)	100	−0.07 ± 0.08
15 (RAN)	790 (270–2300)	117	−0.08 ± 0.04*	570 (250–1300)	192	−0.17 ± 0.01
16 (ZOL)	1000 (420–2400)	93	−0.06 ± 0.08	520 (270–960)	211	−0.12 ± 0.08
17 (TIO)	60 (30–130)	1550	−0.04 ± 0.09	50 (30–90)	2200	−0.12 ± 0.08
18 (FAM)	29 (20–50)	3200	−0.07 ± 0.05	25 (10–40)	4400	−0.14 ± 0.12
19 (APT)	230 (70–760)	404	−0.21 ± 0.05*	290 (160–530)	379	−0.09 ± 0.04

*, $p < 0.05$.

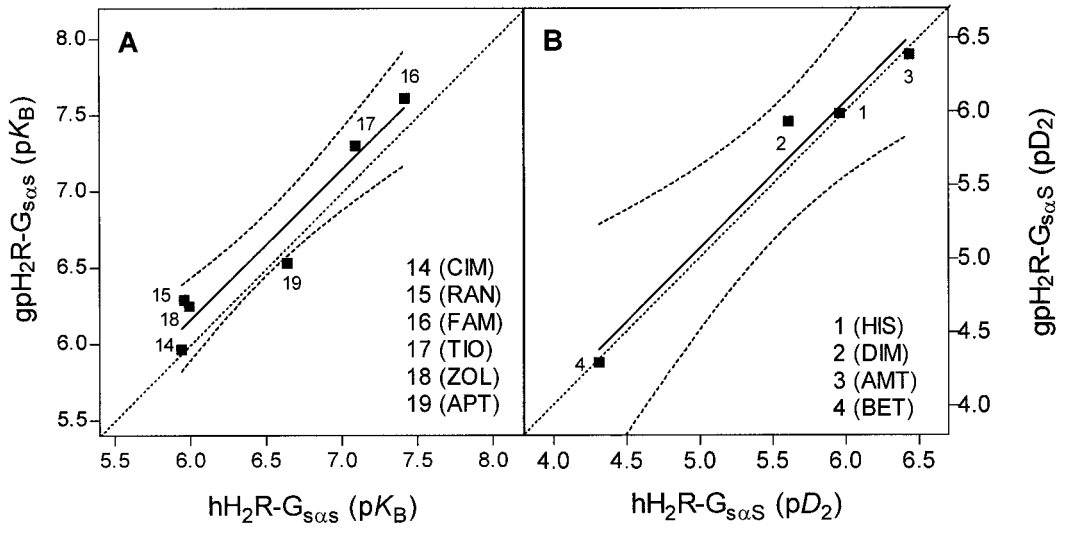

Fig. 5. Relations between pK_B values for antagonists and between pD_2 values for HIS-like agonists at hH_2R-$G_{s\alpha S}$ and gpH_2R-$G_{s\alpha S}$. pK_B values were derived from K_B values shown in Table 1. pD_2 values were derived from EC_{50} values shown in Table 2. Solid lines represent the actual correlations obtained. Dashed lines represent the 95% confidence intervals of the correlations. The straight dotted lines represent the theoretical correlations that would have been obtained if pK_B values and pD_2 values, respectively, had been identical in the two systems compared with each other. The theoretical curves have a slope of 1.00. A, correlation of pK_B values for hH_2R-$G_{s\alpha S}$ versus gpH_2R-$G_{s\alpha S}$. Slope, 0.98 ± 0.13; r^2, 0.94; $p = 0.0015$ (significant). B, correlation of pD_2 values for agonists **1** to **4** at hH_2R-$G_{s\alpha S}$ versus gpH_2R-$G_{s\alpha S}$. Slope, 0.99 ± 0.13; r^2, 0.97; $p = 0.0172$ (significant).

Downloaded from molpharm.aspetjournals.org by guest on December 1, 2012

MOL PHARM

MOLECULAR PHARMACOLOGY

The slope of the correlation between the pD_2 values of guanidines at hH_2R-$G_{s\alpha S}$ and gpH_2R-$G_{s\alpha S}$ was 0.89, and the curve nearly paralleled the theoretical curve assuming pharmacological identity of H_2R species isoforms (Fig. 6B), indicating a constant contribution of the guanidinoalkylaryl moiety to the ligand/GPCR interaction difference between hH_2R and gpH_2R. Notably, agonist potency decreased almost 3-fold at gpH_2R-$G_{s\alpha S}$ by elongation of the alkyl chain between the guanidino group and the phenyl ring (**6** → **7**) (Fig. 1), but slightly increased at hH_2R-$G_{s\alpha S}$. These data indicate that the guanidine binding pocket in gpH_2R is smaller or less flexible than in hH_2R. Taken together, guanidines stabilize an active conformation in gpH_2R not only more efficiently but also more potently than in hH_2R, and the structure-activity relationships for guanidines at hH_2R and gpH_2R are slightly different.

To further corroborate the concept of species-specific H_2R conformations stabilized by guanidines, we competed [^{3}H]TIO binding to H_2R-$G_{s\alpha S}$ fusion proteins with unlabeled guanidines. In the absence of guanine nucleotides, agonist, GPCR, and G-protein form a ternary complex that is characterized by high agonist affinity (Seifert et al., 1998a). Typically, ternary complex formation is not complete; i.e., a certain fraction of GPCRs display low agonist-affinity (Seifert et al., 1998a). Consequently, agonist-competition curves are biphasic. GTPγS reduces agonist affinity, presumably reflecting ternary complex dissociation. However, in some cases, high-affinity agonist binding is GTPγS-insensitive, indicative of tight GPCR/G-protein coupling (Seifert et al., 1998a).

Fig. 7 shows the [^{3}H]TIO competition curves with IMP (**5**), ARP (**8**), and BU-E-48 (**10**) in membranes expressing hH_2R-$G_{s\alpha S}$ and gpH_2R-$G_{s\alpha S}$ in the absence and presence of GTPγS, and Table 3 provides a summary of the nonlinear regression analysis. The K_l-values of guanidines **5**, **8**, and **10** at hH_2R-$G_{s\alpha S}$ were all higher than at gpH_2R-$G_{s\alpha S}$. All K_l values were much more similar to the corresponding EC_{50} in the GTPase assay than the K_h values (Tables 2 and 3). These data suggest that H_2Rs in a conformation with low affinity for guanidines can efficiently mediate GDP/GTP exchange. An explanation for the moderate divergence between K_l and EC_{50} values could be that individual guanidines may interact differently with [^{3}H]TIO-bound and ligand-free H_2R. Dissociations between agonist-affinities in binding assays and agonist potencies in functional assays have been observed for several GPCRs (Wenzel-Seifert et al., 1999; Seifert et al., 2001), and the reader is referred to these articles and references cited therein for a detailed discussion on this topic.

At hH_2R-$G_{s\alpha S}$ and gpH_2R-$G_{s\alpha S}$ the IMP-competition curves in the absence of GTPγS were monophasic (Fig. 7, A and B). GTPγS shifted the IMP-competition curves at both fusion proteins to the right, indicating that despite our inability to resolve high- and low-affinity binding components, IMP still formed a ternary complex with H_2R-$G_{s\alpha S}$. Intriguingly, with gpH_2R-$G_{s\alpha S}$, the IMP-competition curve in the presence of GTPγS was biphasic, suggesting partial stability of the ternary complex of IMP-liganded gpH_2R with GTPγS-liganded $G_{s\alpha S}$. The ternary complex in the hH_2R-$G_{s\alpha S}$ system seems to be less stable as indicated by the monophasic IMP-competition curve in the presence of GTPγS. ARP was highly efficient at stabilizing the ternary complex in both H_2R-$G_{s\alpha S}$ fusion proteins (Fig. 7, C and D). In hH_2R-$G_{s\alpha S}$, GTPγS abolished ternary complex formation with ARP, as reflected by the monophasic and strongly rightward-shifted agonist competition curve (Fig. 7C). In marked contrast, at gpH_2R-$G_{s\alpha S}$, GTPγS had only a small effect on the ARP-competition curve (Fig. 7D), indicating high stability of the ternary complex in the presence of GTPγS-liganded $G_{s\alpha S}$. Similar to ARP, the binding of BU-E-48 (**10**) at hH_2R-$G_{s\alpha S}$ was highly GTPγS-sensitive, and at gpH_2R-$G_{s\alpha S}$ it was largely GTPγS-insensitive (Fig. 7, E and F). Collectively, these data indicate that the conformations of gpH_2R stabilized by guanidines interact more tightly with $G_{s\alpha S}$ than the corresponding conformations of hH_2R. Because of this different GPCR/G-protein interaction, guanidines promote steady-state GDP/GTP exchange through gpH_2R more efficiently than through hH_2R (Fig. 6 and Table 2).

TABLE 2

Agonist efficacies and potencies at hH_2R-$G_{s\alpha S}$ and gpH_2R-$G_{s\alpha S}$ expressed in Sf9 cell membranes

Potencies and efficacies of ligands at hH_2R-$G_{s\alpha S}$ and gpH_2R-$G_{s\alpha S}$ were determined in the GTPase assay. GTP hydrolysis was determined as described under *Experimental Procedures*. Reaction mixtures contained Sf9 membranes expressing fusion proteins and agonists at concentrations from 1 nM to 1 mM as appropriate to generate saturated concentration/response curves. Curves were analyzed by nonlinear regression. Typical basal GTPase activities ranged between ~1 and 2 pmol/mg/min, and typical GTPase activities stimulated by HIS (100 μM) ranged between ~4 and 8 pmol/mg/min. To calculate agonist efficacies, the maximum stimulatory effect of HIS was set at 1.00, and the stimulatory effects of other agonists were referred to this value. Data shown are the means ± SD of four to six experiments performed in duplicate. The relative potency (Rel. Pot.) of HIS was set at 100, and the potencies of other agonists were referred to this value to facilitate comparison of agonist potencies with hH_2R-A271D-$G_{s\alpha S}$, $NgpChH_2R$-$G_{s\alpha S}$, and $NhCgpH_2R$-$G_{s\alpha S}$ (Table 4). Efficacies and potencies, respectively, of ligands at hH_2R-$G_{s\alpha S}$ were compared with the corresponding parameters at gpH_2R-$G_{s\alpha S}$ using the t test.

Compound	hH_2R-$G_{s\alpha S}$			gpH_2R-$G_{s\alpha S}$			EC_{50} hH_2R-$G_{s\alpha S}$/EC_{50} gpH_2R-$G_{s\alpha S}$
	Efficacy	EC_{50}	Rel. Pot.	Efficacy	EC_{50}	Rel. Pot.	
		μM			μM		
1 (HIS)	1.00	1.26 ± 0.25	100	1.00	1.20 ± 0.24	100	1.05
2 (DIM)	0.85 ± 0.07	1.94 ± 0.07*	65.0	0.93 ± 0.04	1.20 ± 0.21	100	1.62
3 (AMT)	0.90 ± 0.06	0.45 ± 0.04	280	1.04 ± 0.05	0.44 ± 0.04	271	1.02
4 (BET)	0.73 ± 0.07	33.6 ± 7.2*	4.00	0.73 ± 0.06	51.4 ± 8.3	2.00	0.65
5 (IMP)	0.84 ± 0.04*	0.20 ± 0.02*	641	1.00 ± 0.12	0.04 ± 0.01	3060	5.00
6 (BU-E-42)	0.86 ± 0.04*	0.42 ± 0.07*	303	1.02 ± 0.08	0.07 ± 0.02	1670	6.00
7 (BU-E-43)	0.56 ± 0.05*	0.28 ± 0.07	448	0.93 ± 0.15	0.19 ± 0.06	631	1.47
8 (ARP)	0.79 ± 0.07*	0.19 ± 0.04*	659	1.02 ± 0.04	0.07 ± 0.01	1600	2.71
9 (BU-E-47)	0.77 ± 0.17*	0.15 ± 0.06*	844	1.07 ± 0.02	0.04 ± 0.00	3030	3.75
10 (BU-E-48)	0.70 ± 0.10*	0.14 ± 0.02*	928	1.00 ± 0.02	0.03 ± 0.00	4080	4.67
11 (BU-E-75)	0.87 ± 0.15	0.33 ± 0.10*	376	1.04 ± 0.03	0.05 ± 0.00	2470	6.60
12 (BU-E-96)	0.78 ± 0.04*	0.31 ± 0.14*	404	0.99 ± 0.08	0.08 ± 0.02	1470	3.88
13 (D281)	0.51 ± 0.14*	0.81 ± 0.13*	155	0.87 ± 0.09	0.21 ± 0.09	570	3.86

*, $p < 0.05$.

Downloaded from molpharm.aspetjournals.org by guest on December 1, 2012

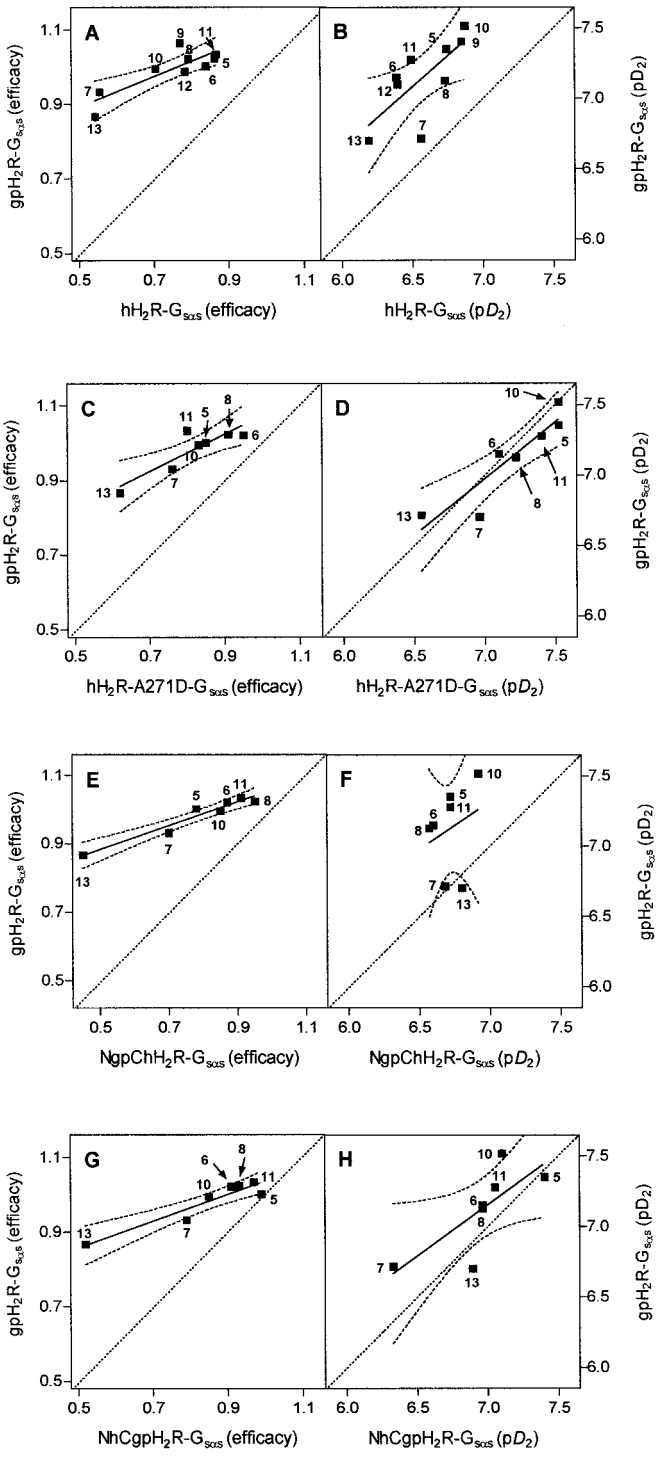

Fig. 6. Relations between efficacies and potencies of guanidines at hH_2R-$G_{s\alpha S}$, hH_2R-A271D-$G_{s\alpha S}$, $NgpChH_2R$-$G_{s\alpha S}$ and $NhCgpH_2R$-$G_{s\alpha S}$, respectively, versus gpH_2R-$G_{s\alpha S}$. Agonist efficacies were taken from Tables 2 and 4, and pD_2 values were derived from the EC_{50} values shown in Tables 2 and 4. Solid lines represent the actual correlations obtained. Dashed lines represent the 95% confidence intervals of the correlations. The straight dotted lines represent the theoretical correlations that would have been obtained if efficacies and pD_2 values, respectively, had been identical in the two systems compared with each other. The theoretical curves have a slope of 1.00. A, correlation of efficacies of agonists **5** to **13** at hH_2R-$G_{s\alpha S}$ versus gpH_2R-$G_{s\alpha S}$. Slope, 0.41 ± 0.10; r^2, 0.72; p = 0.0038 (significant). B, correlation of pD_2 values for agonists **5** to **13** at hH_2R-$G_{s\alpha S}$ versus gpH_2R-$G_{s\alpha S}$. Slope, 0.89 ± 0.32; r^2, 0.53; p = 0.0270 (significant). C, correlation of efficacies of agonists **5** to **8**, **10**, **11**, and **13** at hH_2R-A271D-$G_{s\alpha S}$ versus gpH_2R-$G_{s\alpha S}$. Slope, 0.50 ± 0.12; r^2, 0.77; p = 0.0096 (significant). D, correlation of pD_2 values for agonists **5** to **8**, **10**, **11**, and **13** at hH_2R-A271D-$G_{s\alpha S}$ versus gpH_2R-$G_{s\alpha S}$. Slope, 0.81 ± 0.16; r^2, 0.83; p = 0.0041 (significant). E, correlation of efficacies of agonists **5** to **8**, **10**, **11**, and **13** at $NgpChH_2R$-$G_{s\alpha S}$ versus gpH_2R-$G_{s\alpha S}$. Slope, 0.34 ± 0.04; r^2, 0.94; p = 0.0003 (significant). **F**, correlation of pD_2 values for agonists **5** to **8**, **10**, **11**, and **13** at $NgpChH_2R$-$G_{s\alpha S}$ versus gpH_2R-$G_{s\alpha S}$. Slope, 0.67 ± 1.12; r^2, 0.07; p = 0.57 (not significant). G, correlation of efficacies of agonists **5** to **8**, **10**, **11,** and **13** at $NhCgpH_2R$-$G_{s\alpha S}$ versus gpH_2R-$G_{s\alpha S}$. Slope, 0.36 ± 0.06; r^2, 0.88; p = 0.0015 (significant). H, correlation of pD_2 values for agonists **5** to **8**, **10**, **11**, and **13** at $NhCgpH_2R$-$G_{s\alpha S}$ versus gpH_2R-$G_{s\alpha S}$. Slope, 0.73 ± 0.28; r^2, 0.58; p = 0.0471 (significant).

Molecular Analysis of Guanidine/H_2R Interactions. The crystal structure of bovine rhodopsin (Palczewski et al., 2000) has improved the reliability of GPCR models with bound ligands. To elucidate the structural basis for the differences in interactions of guanidines with H_2R species isoforms, we built three-dimensional models of the seven TM helices of gpH_2R starting from the PDB rhodopsin file 1f88 and using the alignment with the β_2AR (Palczewski et al., 2000). Additionally, our previous 3D QSAR data obtained by comparative molecular field analysis, correlating pD_2 values of guanidines at gpH_2R-atrium with electrostatic and steric field variables, were considered (Dove and Buschauer, 1998, 1999), in particular for defining the conformation and superposition of structures.

Figs. 8 and 9 show the putative binding of IMP (**5**) and ARP (**8**), respectively, to gpH_2R. Presumably, the imidazolylpropylguanidine moiety binds to H_2R like HIS (**1**). Studies with H_2R mutants proved an ionic interaction of the protonated amino group with Asp-98 (TM3) (see also Fig. 2) (Gantz et al., 1992). The second and third site of the widely accepted three-point model for biogenic amine/GPCR interaction could principally be formed by the couples Asp-186/Thr-190 (Gantz et al., 1992) or Tyr-182/Asp-186 in TM5 (Nederkoorn et al., 1996). Based on a pure α-helical TM5, the proposed two hydrogen bonds of the imidazole ring with H_2R are only possible with Tyr-182 and Asp-186. This assumption is also in agreement with a pH-dependent model of H_2R activation that suggests tautomerization of the imidazole into the N_π-H form caused by neutralization of HIS upon binding and accompanied by proton transfers from Tyr-182 to N_π and from N_τ to Asp-186, respectively (Giraldo, 1999). Interactions of nontautomeric agonists with H_2R are compatible with this model, too. Asn-293 of the β_2AR (Wieland et al., 1996) and Phe-436 of the H_1R (Wieland et al., 1999) have been suggested to interact with the β-OH group of epinephrine and with the imidazolylethyl side chain of HIS, respectively. The corresponding residue in TM6 of the H_2R, Phe-254, is near imidazolylpropyl side chain only if agonists do not deeply penetrate into the GPCR core. The selected orientation of the guanidines in Figs. 8 and 9, therefore, is in agreement with our present knowledge on biogenic amine/GPCR interactions.

Disregarding sequence differences deeply within the GPCR core, amino acid exchanges between hH_2R and gpH_2R occur only on the top of TM1 and TM7. Direct IMP- and ARP-TM1 interaction is impossible. However, the minimized gpH_2R models consistently result in an interhelical TM1–TM7 H-bond between Tyr-17 (hH_2R: Cys-17) and Asp-271. In TM7, there are three amino acid differences between hH_2R and gpH_2R (Leu-269 → Phe-269, Ala-271 → Asp-271, and Ile-272 → Val-272) (Fig. 2). With our rhodopsin-based alignment of TM7, only Asp-271 is capable of directly participating in

MOL PHARM
MOLECULAR PHARMACOLOGY
aspet
Downloaded from molpharm.aspetjournals.org by guest on December 1, 2012

ligand binding. Intriguingly, the Ala-271→Asp-271 switch is the only nonconserved amino acid exchange between hH_2R and gpH_2R in TM7. The model in Fig. 8 suggests that the preference of IMP for gpH_2R relative to hH_2R is caused by an H-bond of the $N_\tau H$ function to Asp-271. For the pyridyl moiety of ARP, an ion-dipole interaction with Asp-271 is possible (Fig. 9) in agreement with our 3D QSAR results (Dove and Buschauer, 1998, 1999), indicating that a positive charge in

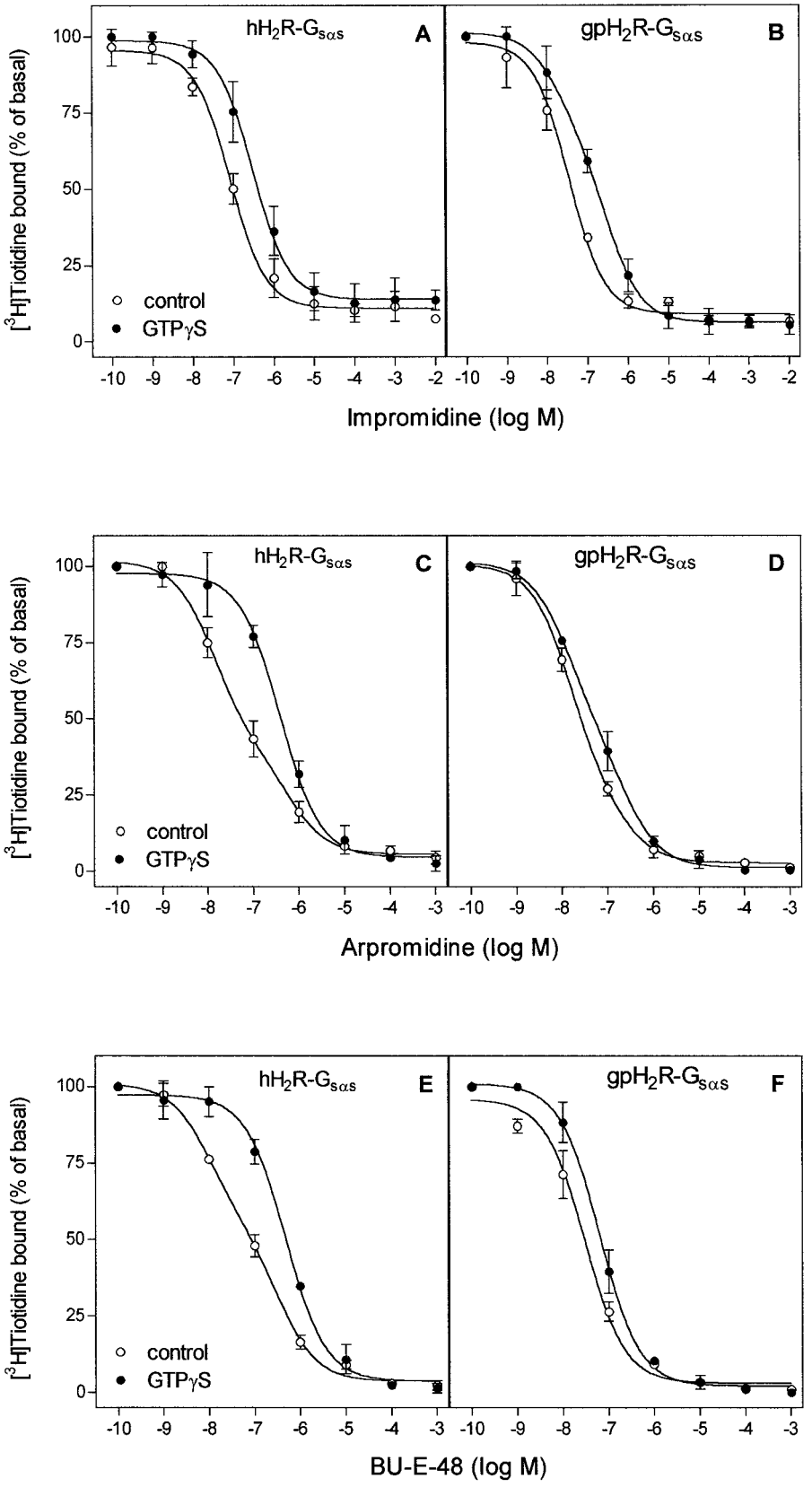

Fig. 7. Competition of [^{3}H]TIO binding by guanidines in Sf9 membranes expressing hH_2R-$G_{s\alpha S}$ and gpH_2R-$G_{s\alpha S}$. [^{3}H]TIO binding in Sf9 membranes was performed as described under *Experimental Procedures*. Reaction mixtures contained membranes expressing fusion proteins, 10 nM [^{3}H]TIO and agonists at the concentrations indicated on the *abscissa*. Reaction mixtures additionally contained distilled water (control) or GTPγS (10 μM). A and B, IMP (**5**); C and D, ARP (**8**); E and F, BU-E-48 (**10**). Data were analyzed for best fit to monophasic or biphasic competition curves (F test). Data shown are the means ± S.D. of three to five experiments performed in duplicate.

MOL PHARM
MOLECULAR PHARMACOLOGY
aspet
Downloaded from molpharm.aspetjournals.org by guest on December 1, 2012

MOL PHARM

TABLE 3

Binding properties of guanidines at $hH_2R\text{-}G_{s\alpha S}$ and $gpH_2R\text{-}G_{s\alpha S}$ expressed in Sf9 cell membranes

Agonist competition binding was determined as described under *Experimental Procedures*. The data shown in Fig. 7 were analyzed by nonlinear regression for best fit to monophasic or biphasic competition curves. Data shown are the means of four to six experiments performed in duplicate. Numbers in parentheses represent the 95% confidence intervals. K_h and K_l designate the dissociation constants for the high- and low-affinity state of H_2Rs, respectively. $\%R_h$ indicates the percentage of high-affinity binding sites. The corresponding values obtained in the presence of GTPγS (10 μM) are referred to as $K_{hGTP\gamma S}$, $K_{lGTP\gamma S}$ and $\%R_{hGTP\gamma S}$, respectively. If data were best fit to monophasic competition curves, data are listed under K_l and $K_{lGTP\gamma S}$, respectively.

Agonist	K_h	K_l	$\%R_h$	$K_{hGTP\gamma S}$	$K_{lGTP\gamma S}$	$\%R_{hGTP\gamma S}$
	nM			*nM*		
$hH_2R\text{-}G_{s\alpha S}$						
5 (IMP)		64 (48–85)			234 (167–327)	
8 (ARP)	11 (6.2–18)	461 (200–1055)	63.7 (50.7–76.8)		296 (216–404)	
10 (BU-E-48)	7.2 (3.4–15.5)	248 (129–475)	46.0 (31.8–60.3)		368 (288–469)	
$gpH_2R\text{-}G_{s\alpha S}$						
5 (IMP)		27 (21–36)		14.4 (3.4–62)	236 (109–510)	33.2 (5.8–60.7)
8 (ARP)	12 (5.6–25)	152 (5–4700)	78.4 (33.6–123.1)	10 (3.6–28)	164 (43–627)	53.3 (19.6–87.1)
10 (BU-E-48)	0.02 (0.01–0.08)	31 (20–47)	43.9 (14.5–67.9)		49 (41–60)	

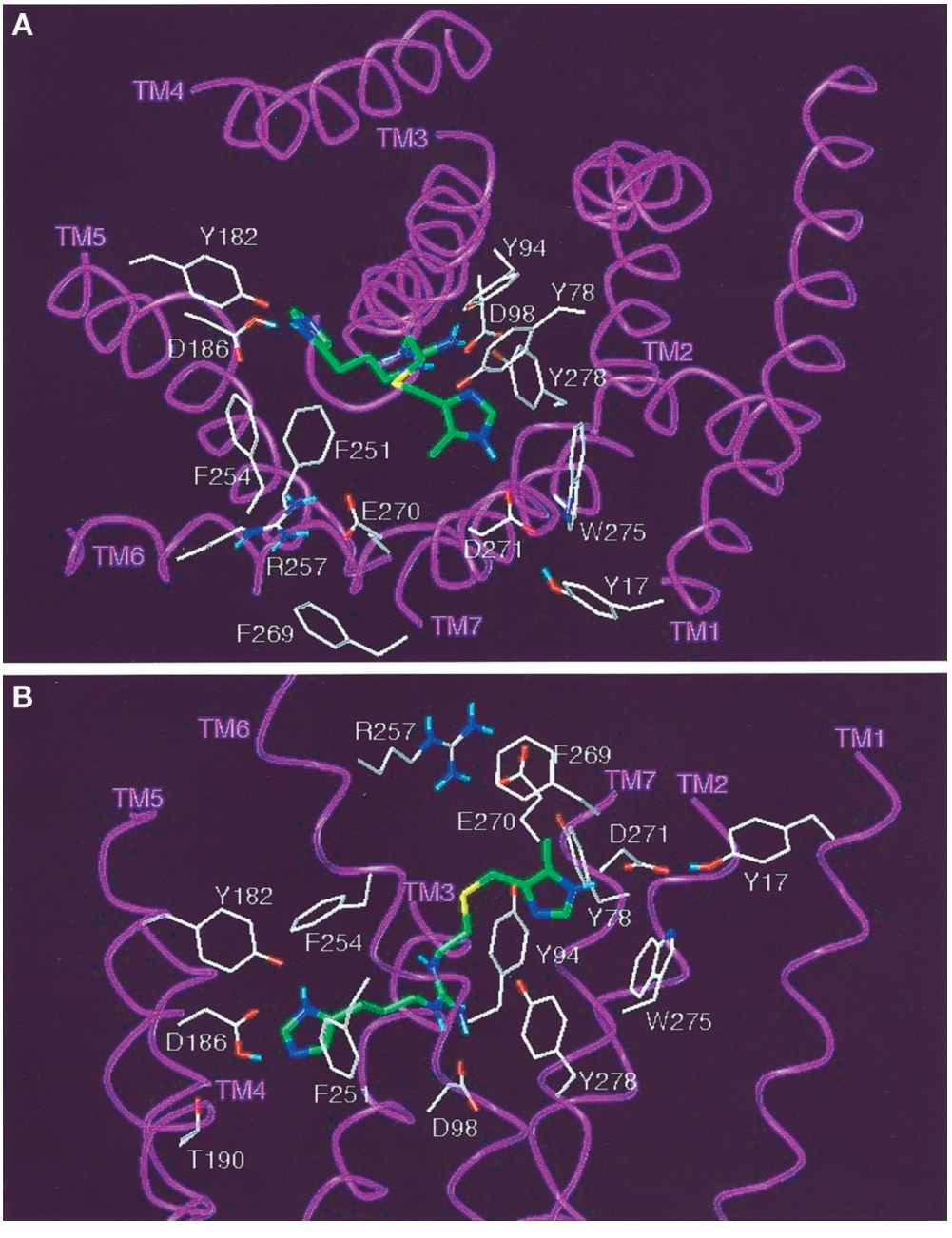

Fig. 8. Model of the interaction of IMP with the gpH_2R. The carbon atoms of IMP (**5**) are shown in green. Side chains and α-carbon atoms of the putative agonist-binding site and at the top of TM1 and TM7 are drawn. A, view into the GPCR core; B, lateral view. The imidazolylpropylguanidine moiety interacts with Asp-98 in TM3 (Gantz et al., 1992) and the Tyr-182/Asp-186 pair in TM5 (Nederkoorn et al., 1996). Asn-293 of the β_2AR (Wieland et al., 1996) and Phe-436 of the H_1R (Wieland et al., 1999) have been suggested to interact with the β-OH group of epinephrine and with the imidazolylethyl side chain of HIS, respectively. The corresponding residue of the H_2R, Phe-254, is close to the imidazolylpropyl side chain only if agonists do not deeply penetrate into the GPCR core. Major differences in amino acid sequence between hH_2R and gpH_2R occur on the top of TM1 and TM7. The gpH_2R model proposes H-bonds of Asp-271 (hH_2R: Ala-271) in TM7 to the N_τ hydrogen of the 5-methyl-1*H*-imidazol-4-yl group of IMP and to the OH group of Tyr-17 (hH_2R: Cys-17) in TM1. Because of the different amino acid substitutions in hH_2R, these H-bonds are not possible in this GPCR.

MOLECULAR PHARMACOLOGY

aspet

Downloaded from molpharm.aspetjournals.org by guest on December 1, 2012

the pyridyl region increases potency at gpH_2R. Ala-271 in hH_2R cannot take part in these H-bond and ion-dipole interactions.

To test the predictions of the 3D QSAR and computer modeling studies, we constructed hH_2R-A271D-$G_{s\alpha S}$ in which Ala-271 is exchanged against Asp-271 (Fig. 10A). Ad-

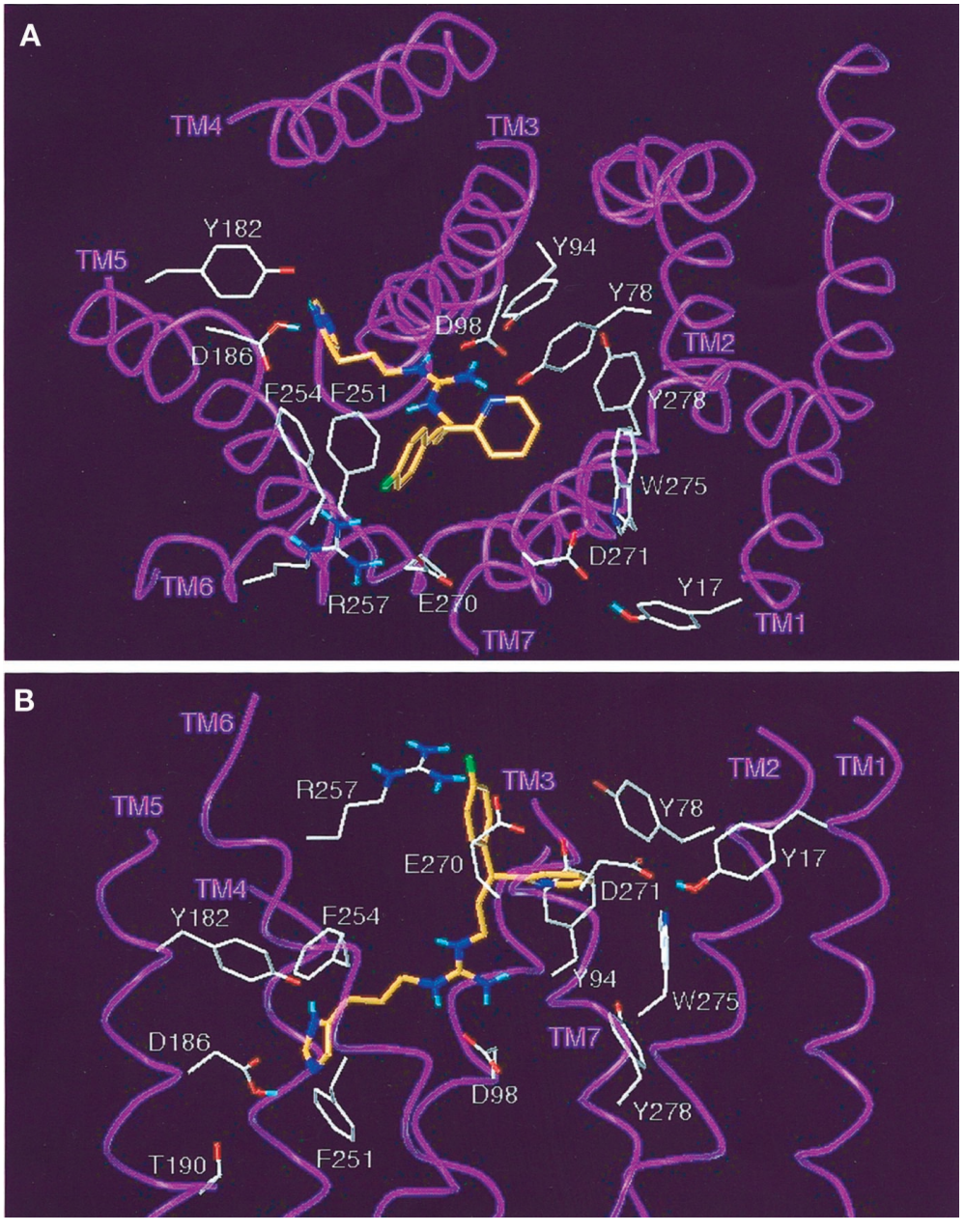

Fig. 9. Model of the interaction of ARP with the gpH_2R. The carbon atoms of ARP (**8**) are shown in orange. Side chains and α-carbon atoms of the putative agonist-binding site and at the top of TM1 and TM7 are drawn. A, view into the GPCR core; B, lateral view. For description of the binding of the imidazolylpropyl moiety, see Fig. 8. Asp-271 (hH_2R: Ala-271) in TM7 again forms an H-bond to the OH group of Tyr-17 (hH_2R: Cys-17) in TM1. For most favorable interaction with the H_2R, the pyridyl- and the phenyl group must be arranged as shown. Attempts to roughly exchange the position of both rings by rotation of the propyl side chain bonds either resulted in high-energy conformations or in collision with the helices. Significantly different QSAR with respect to substituents at the phenyl ring of derivatives of ARP (**8**) and of unbranched phenyl as well as benzylthioalkyl compounds, respectively, suggest that the aryl or heteroaryl ring of structures such as IMP must be superimposed with the pyridyl ring of the pyridylphenylpropyl analogs. In particular, bulk is unfavorable for potency around the "pyridyl site" and allowed in *meta* and *para* position of the "phenyl site". This agrees with a model where the latter site points outside the GPCR core. The suggested binding mode of the "pyridyl site" of ARP derivatives further considers that 2- and 3-pyridylphenylpropyl structures are on average 0.3 to 0.4 pD_2 units more potent than the corresponding diphenyl analogs. The model in Fig. 9 assumes the pyridyl group of ARP to be surrounded by a pocket of the aromatic residues Tyr-78, Tyr-94, Trp-275, and Tyr-278, where ligand bulk is restricted. Corresponding to Tyr-78, His-93 of the β_2AR is probably involved in the binding of the *p*-methoxy group of formoterol (Isogaya et al., 1999). One of these hydrogen-donating aromatic residues might form an H-bond with the pyridyl nitrogen of ARP, but the model rather suggests an ion-dipole interaction of Asp-271 with a positively charged region of the pyridyl group. Studies with β_2AR mutants (Isogaya et al., 1999) point to an interaction of Tyr-308, corresponding to Glu-270 in H_2Rs, with the arylalkyl side chain of formoterol. In the gpH_2R model, a salt bridge between Glu-270 and Arg-257 (TM6) positions both side chains for additional interaction with the phenyl moiety of ARP. In agreement with our 3D QSAR studies, indicating favorable effects of negatively charged *meta* and *para* substituents, ion-dipole interactions or, as anticipated in the case of ARP, a F—HN H-bond with Arg-257 could be possible. The field effect of Arg-257 might additionally amplify interactions of Glu-270 with positively charged phenyl regions.

MOL PHARM
MOLECULAR PHARMACOLOGY
aspet
Downloaded from molpharm.aspetjournals.org by guest on December 1, 2012

MOL PHARM

MOLECULAR PHARMACOLOGY

ditionally, we took advantage of a *Kpn*I site present in the cDNA of both hH_2R and gpH_2R (Fig. 2). *Kpn*I cleaves the cDNAs of hH_2R and gpH_2R at the same position localized in the middle of the second intracellular loop (Fig. 2). Thus, we could readily construct chimeras in which the N- and C-terminal portions of hH_2R and gpH_2R were exchanged against each other (Fig. 10A). $NhCgpH_2R$-$G_{s\alpha}$ bears Cys-17 and Asp-271, and $NgpChH_2R$-$G_{s\alpha}$ bears Tyr-17 and Ala-271. The chimeras could be used 1) to study the role of Asp-271/Ala-271 in the interaction with guanidines and 2) to study the importance of the suggested H-bond between Tyr-17 and Asp-271 for the effects of guanidines at gpH_2R. In hH_2R-$G_{s\alpha}$, both chimeras and hH_2R-A271D-$G_{s\alpha}$ this interaction cannot take place anymore because either of the two amino acids is replaced (Fig. 1).

Immunoblots with the anti-FLAG Ig showed that hH_2R-A271D-$G_{s\alpha S}$, $NgpChH_2R$-$G_{s\alpha S}$, and $NhCgpH_2R$-$G_{s\alpha S}$, like hH_2R-$G_{s\alpha S}$ and gpH_2R-$G_{s\alpha S}$, had a molecular mass of ~78 kDa (Fig. 10B). The expression levels of the membrane preparations shown in Fig. 10 were quite different, but this does not reflect intrinsic differences in the expression levels of constructs. Specifically, Fig. 3 contains immunoblots in which hH_2R-$G_{s\alpha S}$ and gpH_2R-$G_{s\alpha S}$ were expressed at higher levels than in those displayed in Fig. 10, and similar data were obtained for $NhCgpH_2R$-$G_{s\alpha S}$ (data not shown). Membranes with different expression levels were intentionally chosen for the immunoblot in Fig. 10 because certain features, namely the double bands of H_2R-$G_{s\alpha}$ fusion proteins corresponding to differently glycosylated species (Liu et al., 2001), become much more obvious with constructs at low expression levels. The immunoblot with the anti-FLAG Ig also shows the dimers of $NgpChH_2R$-$G_{s\alpha S}$ and hH_2R-A271D-$G_{s\alpha S}$ migrating at ~160 kDa. The immunoblot with anti-$G_{s\alpha}$ Ig confirmed that H_2R-$G_{s\alpha}$ fusion proteins migrate as a monomer of ~78 kDa and a dimer of ~160 kDa (Fig. 10C). Three additional bands at ~50 to 60 kDa not identified with the anti-FLAG Ig are seen in the immunoblot with anti-$G_{s\alpha}$. They do not correspond to the endogenous $G_{s\alpha}$-like G-protein of insect cells because the anti-$G_{s\alpha}$ Ig did not recognize an antigen in membranes from uninfected Sf9 cells (Fig. 10C). The bands also do not represent degradation products since the immunoblot with the anti-FLAG Ig did not provide an indication (compare also with the partial degradation of β_2AR-$G_{s\alpha L}$ shown in Fig. 3). Rather, we assume that the ~50- to 60-kDa proteins are atypically migrating H_2R-$G_{s\alpha}$ fusion proteins that, because of specific N-terminal glycosylation patterns, are recognized only by the C-terminally reacting anti-$G_{s\alpha}$ Ig but not with the N-terminally reacting anti-FLAG Ig. Glycosylation-dependent reactions of fusion proteins with anti-FLAG Ig and anti-$G_{s\alpha}$ Ig and atypical migrations of GPCRs in SDS-PAGE have been observed earlier (Grünewald et al., 1996; Liu et al., 2001). Collectively, the immunoblots with the anti-FLAG Ig and anti-$G_{s\alpha}$ Ig show that hH_2R-A271D-$G_{s\alpha S}$, $NgpChH_2R$-$G_{s\alpha S}$, and $NhCgpH_2R$-$G_{s\alpha S}$ are expressed in Sf9 cell membranes and that the electrophoretic mobility of those fusion proteins is similar to the mobility of fusion proteins containing wild-type H_2Rs.

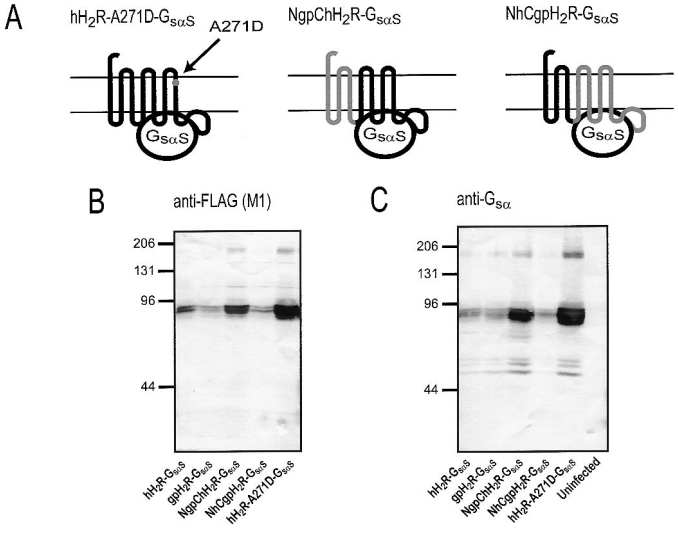

Fig. 10. Analysis of the expression of hH_2R-A271D-$G_{s\alpha S}$, $NgpChH_2R$-$G_{s\alpha}$ and $NhCgpH_2R$-$G_{s\alpha}$ fusion proteins in Sf9 cell membranes. A, schematic structures of hH_2R-A271D-$G_{s\alpha S}$, $NgpChH_2R$-$G_{s\alpha}$ and $NhCgpH_2R$-$G_{s\alpha}$ fusion proteins. For precise location of the *Kpn*I site used for construction of chimeras, see Fig. 2. Sf9 cell membranes expressing various H_2R-$G_{s\alpha}$ fusion proteins or membranes from uninfected Sf9 cells were separated by SDS-PAGE using a gel that contained 8% (w/v) acrylamide. Fusion proteins were probed with the anti-FLAG Ig (M1 antibody) (B) or the anti-$G_{s\alpha}$ Ig (C). For each membrane preparation, 100 μg of protein was applied to each lane. Numbers on the left of the immunoblots indicate molecular masses of marker proteins. Shown are the horseradish peroxidase-reacted Immobilon *P* membranes of representative gels. Similar results were obtained with two other membrane preparations of hH_2R-A271D-$G_{s\alpha S}$, $NgpChH_2R$-$G_{s\alpha}$, and $NhCgpH_2R$-$G_{s\alpha}$ fusion proteins.

Table 4 summarizes the potencies and efficacies of HIS (**1**) and guanidines **5** to **8**, **10**, **11**, and **13** at the GTPase of hH_2R-A271D-$G_{s\alpha S}$, $NgpChH_2R$-$G_{s\alpha S}$, and $NhCgpH_2R$-$G_{s\alpha S}$. Figure 6, C-H, shows correlations of the efficacies and potencies, respectively of guanidines at hH_2R-A271D-$G_{s\alpha S}$, $NgpChH_2R$-$G_{s\alpha S}$ and $NhCgpH_2R$-$G_{s\alpha S}$, respectively, versus gpH_2R-$G_{s\alpha S}$ and allow direct comparison with the properties of hH_2R-$G_{s\alpha S}$ versus gpH_2R-$G_{s\alpha S}$ (Fig. 6, A and B). Most strikingly, the correlation between the pD_2 values of guanidines at hH_2R-A271D-$G_{s\alpha S}$ and gpH_2R-$G_{s\alpha S}$ almost exactly followed the theoretical curve assuming pharmacological identity of the two fusion proteins (Fig. 6D). Thus, the Ala-271 → Asp-271 mutation increased the potency of hH_2R for guanidines to the level of gpH_2R (compare Fig. 6, B and D, and Tables 2 and 4). These findings confirm the results of the 3D QSAR (Dove and Buschauer, 1998, 1999) and modeling studies (Figs. 8 and 9) suggesting that the potency of guanidines is increased by ion-dipole or H-bond interactions with Asp-271. Such interactions cannot occur with Ala-271 in hH_2R, which explains why at hH_2R guanidines exhibit substantially lower potencies than at gpH_2R (compare Fig. 6, B and D).

The chimera $NgpChH_2R$-$G_{s\alpha S}$ contains Ala-271 (Figs. 1 and 10A). As expected, the potencies of guanidines at $NgpChH_2R$-$G_{s\alpha S}$ did not approach the theoretical curve assuming pharmacological identity of $NgpChH_2R$-$G_{s\alpha S}$ and gpH_2R-$G_{s\alpha S}$ (Fig. 6F). Like hH_2R-A271D-$G_{s\alpha S}$, $NhCgpH_2R$-$G_{s\alpha S}$ contains Asp-271. Thus, the potencies of guanidines at $NhCgpH_2R$-$G_{s\alpha S}$ were expected to be higher than at hH_2R-$G_{s\alpha S}$ and similar to the potencies at hH_2R-A271D-$G_{s\alpha S}$ and gpH_2R-$G_{s\alpha S}$. Overall, the data fulfilled the predictions (Tables 2 and 4). As a result of the increase in guanidine potency at $NhCgpH_2R$-$G_{s\alpha S}$ the correlation between the pD_2 values at $NhCgpH_2R$-$G_{s\alpha S}$ versus gpH_2R-$G_{s\alpha S}$ approached the theoretical function assuming pharmacological identity (compare Fig. 6, B and H), but not as close as in the case of hH_2R-

Downloaded from molpharm.aspetjournals.org by guest on December 1, 2012

MOL PHARM

MOLECULAR PHARMACOLOGY

A271D-$G_{s\alpha S}$ versus gpH_2R-$G_{s\alpha S}$ (compare Figs. 6, D and H). Such slightly reduced potencies were not unexpected, because in $NhCgpH_2R$-$G_{s\alpha S}$, there is not only the Ala-271 → Asp-271 exchange, but also 32 additional amino acid exchanges in various regions of the C-terminal half of the GPCR (Fig. 2). These exchanges can have multiple effects on the arrangements of TM domains and thereby partially annihilate the effect of the Ala-271 → Asp-271 exchange on guanidine potency.

Regarding the properties of some specific agonists, it becomes obvious that elongation of the alkyl chain between the guanidino group and the phenyl ring (**6** → **7**) (Fig. 1) decreased agonist potency at hH_2R-A271D-$G_{s\alpha S}$ and $NhCgpH_2R$-$G_{s\alpha S}$ by ~4-fold (Table 4). This decrease in potency is similar to that observed for compounds **6**→**7** at gpH_2R-$G_{s\alpha S}$ (Table 2). Conversely, at $NgpChH_2R$-$G_{s\alpha S}$ and hH_2R-$G_{s\alpha S}$ the longer alkyl chain slightly increased agonist potency (Tables 2 and 4). These data indicate that the amino acid at position 271 of H_2R affects the size and flexibility of the guanidine binding pocket. With Ala-271, the binding pocket is wider and more flexible and accommodates the longer (**7**) as well as the shorter guanidine (**6**). In contrast, with Asp-271, the fit of the longer guanidine (**7**) must be probably enforced by conformational strain.

Among all guanidines studied, the amino acid substitution at position 271 had the greatest and most consistent impact on the potency of IMP (**5**). Specifically, with Asp-271 the potencies of IMP were consistently ~5- to 7-fold higher than with Ala-271, regardless of whether fusion proteins with wild-type H_2Rs, mutated H_2R, or chimeric H_2Rs were considered (Tables 2 and 4). For other guanidines, the impact of the amino acid substitution at position 271 was less consistent. These data indicate that the binding of IMP to H_2R is considerably more dependent on interaction with Asp-271 than the binding of other guanidines to H_2R. Major structural features of IMP (**5**) compared with the other guanidines studied (**6**–**13**) are the possibility of a H-bond to Asp-271 (see Fig. 8) and the absence of a phenyl branch (Fig. 1). In the case of the guanidines **6**–**13**, the weaker ion-dipole interaction with Asp-271 may be compensated by electrostatic interactions of the substituted phenyl group with Arg-257 and Glu-270 and by better fit of the pyridyl moiety into a pocket of aromatic residues (see Fig. 9).

Another striking result of the studies with hH_2R-A271D-$G_{s\alpha S}$, $NgpChH_2R$-$G_{s\alpha S}$, and $NhCgpH_2R$-$G_{s\alpha S}$ was that the correlations of the efficacies of guanidines at the aforementioned constructs versus gpH_2R-$G_{s\alpha S}$ remained almost unchanged (Fig. 6, A, C, E, and G), indicating that neither Asp-271 nor all 33 amino acids specific for the C-terminal half of gpH_2R restored high efficacy of guanidines observed for gpH_2R-$G_{s\alpha S}$. These data demonstrate that guanidine potency and efficacy are independent H_2R properties. Intriguingly, the models in Figs. 8 and 9 point to the existence of a H-bond between Tyr-17 and Asp-271, a couple of residues present only in gpH_2R-$G_{s\alpha S}$. Thus, our modeling and experimental data suggest that the Tyr-Asp H-bond stabilizes the agonistic conformation of the gpH_2R bound to guanidines.

It was also surprising that HIS is 2- to 3.5-fold *more potent* at hH_2R-A271D-$G_{s\alpha S}$ and $NhCgpH_2R$-$G_{s\alpha S}$ (both with Cys-17 and Asp-271) than at gpH_2R-$G_{s\alpha S}$ (Tables 2 and 4). TM1 and TM7 do not belong to the binding site of HIS, although it cannot be ruled out that an unfixed Asp side chain in a more flexible TM7 can slightly improve the association kinetics of small amines by "dynamic escorting".

Conclusions

In previous studies we observed that several guanidine-type H_2R agonists are less potent and/or less efficient at the H_2R of human neutrophils than at the H_2R of the guinea pig atrium (Burde et al., 1989, 1990; Buschauer, 1989). Taking advantage of the cloned hH_2R and gpH_2R (Gantz et al., 1991; Traiffort et al., 1995) and the GPCR-G_α fusion protein technique (Seifert et al., 1999; Milligan, 2000) we were able to analyze the coupling of hH_2R and gpH_2R to $G_{s\alpha S}$ under identical experimental conditions. Using this approach, we have dissected pharmacological differences between hH_2R and gpH_2R with respect to the inverse agonist efficacies of RAN (**16**) and APT (**19**) and the agonist potencies and efficacies of guanidines **5**–**13**. Thus, our present data clearly show that hH_2R and gpH_2R possess, indeed, different pharmacological properties.

TABLE 4

Agonist efficacies and potencies at hH_2R-A271D-$G_{s\alpha S}$, $NgpChH_2R$-$G_{s\alpha S}$, and $NhCgpH_2R$-$G_{s\alpha S}$ expressed in Sf9 cell membranes

Potencies and efficacies of ligands at hH_2R-A271D-$G_{s\alpha S}$, $NgpChH_2R$-$G_{s\alpha S}$, and $NhCgpH_2R$-$G_{s\alpha S}$ were determined in the GTPase assay. GTP hydrolysis was determined as described under *Experimental Procedures*. Reaction mixtures contained Sf9 membranes expressing fusion proteins and agonists at concentrations from 1 nM to 1 mM as appropriate to generate saturated concentration/response curves. Curves were analyzed by nonlinear regression. Typical basal GTPase activities ranged between ~1 and 2 pmol/mg/min, and typical GTPase activities stimulated by HIS (100 μM) ranged between ~4 and 8 pmol/mg/min. To calculate agonist efficacies, the maximum stimulatory effect of HIS was set at 1.00, and the stimulatory effects of other agonists were referred to this value. Data shown are the means ± S.D. of three to six experiments performed in duplicates. The relative potency (Rel. Pot.) of HIS was set at 100, and the potencies of other agonists were referred to this value to facilitate comparison of agonist potencies with hH_2R-$G_{s\alpha S}$ and gpH_2R-$G_{s\alpha S}$ (Table 2).

Compound	hH_2R-A271D-$G_{s\alpha S}$			$NgpChH_2R$-$G_{s\alpha S}$			$NhCgpH_2R$-$G_{s\alpha S}$		
	Efficacy	EC_{50}	Rel. Pot.	Efficacy	EC_{50}	Rel. Pot.	Efficacy	EC_{50}	Rel. Pot.
		μM			μM			μM	
1 (HIS)	1.00	0.35 ± 0.05	100	1.00	1.98 ± 0.67	100	1.00	0.71 ± 0.26	100
5 (IMP)	0.85 ± 0.12	0.03 ± 0.01	1300	0.78 ± 0.10	0.19 ± 0.03	1040	0.99 ± 0.09	0.04 ± 0.01	1780
6 (BU-E-42)	0.95 ± 0.08	0.08 ± 0.01	438	0.87 ± 0.02	0.25 ± 0.04	792	0.91 ± 0.02	0.11 ± 0.03	645
7 (BU-E-43)	0.76 ± 0.09	0.28 ± 0.04	125	0.70 ± 0.03	0.21 ± 0.03	943	0.79 ± 0.01	0.46 ± 0.03	154
8 (ARP)	0.91 ± 0.04	0.06 ± 0.01	583	0.95 ± 0.06	0.27 ± 0.04	733	0.93 ± 0.06	0.11 ± 0.05	645
10 (BU-E-48)	0.83 ± 0.04	0.03 ± 0.00	1170	0.85 ± 0.03	0.12 ± 0.02	1650	0.85 ± 0.03	0.08 ± 0.02	888
11 (BU-E-75)	0.80 ± 0.10	0.04 ± 0.01	875	0.91 ± 0.06	0.19 ± 0.01	1040	0.97 ± 0.05	0.09 ± 0.01	789
13 (D281)	0.62 ± 0.11	0.11 ± 0.02	318	0.45 ± 0.06	0.16 ± 0.05	1240	0.52 ± 0.14	0.13 ± 0.04	546

aspet

Downloaded from molpharm.aspetjournals.org by guest on December 1, 2012

Guanidines stabilize an active conformation in gpH_2R more efficiently and potently than in hH_2R. Site-directed mutagenesis studies and analysis of chimeric hH_2R/gpH_2R receptors confirmed computer modeling proposing that Asp-271 accounts for the high potency of guanidines. The gpH_2R model also suggests that high guanidine efficacy depends on an H-bond between Asp-271 and Tyr-17 that is not possible in any other H_2R-$G_{s\alpha}$ construct studied. Thus, our data show that hH_2R and gpH_2R selectively interact with a single class of synthetic agonists, that high guanidine potency critically depends on interaction with a single single amino acid, and that agonist potency and efficacy are regulated independently of each other. The inverse order of potency of compounds **6** and **7** at hH_2R and gpH_2R, respectively, indicates that it is possible to develop guanidines with potency at hH_2R. Such compounds may be useful for treating cardiac failure, acute myelogenous leukemia, and inflammatory diseases.

Our present study adds the H_2R to the growing list of GPCR species isoforms that interact similarly with their endogenous ligand, but quite differently with synthetic ligands (Kopin et al., 2000; Ligneau et al., 2000; Lovenberg et al., 2000). Many GPCR species isoforms, including the H_3R, differ from each other primarily in antagonist pharmacology (Kopin et al., 2000; Ligneau et al., 2000; Lovenberg et al., 2000). From a historical perspective, it is very fortunate that the pharmacological differences between hH_2R and gpH_2R mainly concern agonists and not antagonists (Fig. 5). Otherwise, it would have been much more difficult if not impossible to develop potent H_2R antagonists for treatment of gastroduodenal ulcer disease in man relying on animal models at a time when recombinant hH_2R had not yet been available. However, for future development of potent and selective H_2R agonists it will be crucial to analyze hH_2R and not gpH_2R.

Acknowledgments

We thank Dr. I. Gantz (Ann Arbor, MI) for providing the cDNA of hH_2R, Drs. E. Traiffort and J.-C. Schwartz (Paris, France) for providing the cDNA of gpH_2R and Dr. F. Schalkhausser (Department of Pharmacy, University of Regensburg, Germany) for the synthesis of guanidine **13**. We also thank Dr. U. Gether (Department of Medical Physiology, The Panum Institute, Copenhagen, Denmark) for stimulating discussions. Finally, we thank the reviewers for their very helpful critique and suggestions.

References

Alewijnse AE, Smit MJ, Hoffmann M, Verzijl D, Timmerman H, and Leurs R (1998) Constitutive activity and structural instability of the wild-type human H_2 receptor. *J Neurochem* **71:**799–807.

Burde R, Buschauer A, and Seifert R (1990) Characterization of histamine H_2-receptors in human neutrophils with a series of guanidine analogues of impromidine. Are cell type-specific H_2-receptors involved in the regulation of NADPH oxidase? *Naunyn-Schmiedeberg's Arch Pharmacol* **341:**455–461.

Burde R, Seifert R, Buschauer A, and Schultz G (1989) Histamine inhibits activation of human neutrophils and HL-60 leukemic cells via H_2-receptors. *Naunyn-Schmiedeberg's Arch Pharmacol* **340:**671–678.

Buschauer A (1989) Synthesis and in vitro pharmacology of arpromidine and related phenyl(pyridylalkyl)guanidines, a potential new class of positive inotropic drugs. *J Med Chem* **32:**1963–1970.

Chidiac P, Nouet S, and Bouvier M (1996) Agonist-induced modulation of inverse agonist efficacy at the β_2-adrenergic receptor. *Mol Pharmacol* **50:**662–669.

Dove S and Buschauer A (1998) Imidazolylpropylguanidines as histamine H_2 receptor agonists: 3D-QSAR of a large series. *Pharm Acta Helv* **73:**145–155.

Dove S and Buschauer A (1999) Improved alignment by weighted field fit in CoMFA of histamine H_2 receptor agonistic imidazolylpropylguanidines. *Quant Struct Act Relat* **18:**329–341.

Durant GJ, Duncan WA, Ganellin CR, Parsons ME, Blakemore RC, and Rasmussen AC (1978) Impromidine (SK&F 92676) is a very potent and specific agonist for histamine H_2 receptors. *Nature (Lond)* **276:**403–405.

Felix SB, Buschauer A, and Baumann G (1995) Haemodynamic profile of new H_2-receptor agonists in congestive heart failure. *Eur J Clin Invest* **25(Suppl 1):**42–46.

Fukushima Y, Asano T, Saitoh T, Anai M, Funaki M, Ogihara T, Katagiri H, Matsuhashi N, Yazaki Y, and Sugano K (1997) Oligomer formation of histamine H_2 receptors expressed in Sf9 and COS7 cells. *FEBS Lett* **409:**283–286.

Gajtkowski GA, Norris DB, Rising TJ, and Wood TP (1983) Specific binding of ^{3}H-tiotidine to histamine H_2 receptors in guinea pig cerebral cortex. *Nature (Lond)* **304:**65–67.

Ganellin CR (1982) Chemistry and structure-activity relationships of drugs acting at histamine receptors, in *Pharmacology of Histamine Receptors* (Ganellin CR and Parsons ME eds) pp 10–102, Wright-PSG, Bristol, England.

Gantz I, Munzert G, Tashiro T, Schaffer M, Wang L, DelValle J, and Yamada T (1991) Molecular cloning of the human histamine H_2 receptor. *Biochem Biophys Res Commun* **178:**1386–1392.

Gantz I, DelValle J, Wang LD, Tashiro T, Munzert G, Guo YJ, Konda Y, and Yamada T (1992) Molecular basis for the interaction of histamine with the histamine H_2 receptor. *J Biol Chem* **267:**20840–20843.

Giraldo J (1999) A pH-dependent model of the activation mechanism of the histamine H_2 receptor. *Biochem Pharmacol* **58:**343–353.

Grünewald S, Haase W, Reiländer H, and Michel H (1996) Glycosylation, palmitoylation, and localization of the human D_{2S} receptor in baculovirus-infected insect cells. *Biochemistry* **35:**15149–15161.

Hill SJ, Ganellin CR, Timmerman H, Schwartz JC, Shankley NP, Young JM, Schunack W, Levi R, and Haas HL (1997) International Union of Pharmacology. XIII. Classification of histamine receptors. *Pharmacol Rev* **49:**253–278.

Hirschfeld J, Buschauer A, Elz S, Schunack W, Ruat M, Traiffort E, and Schwartz JC (1992) Iodoaminopotentidine and related compounds: a new class of ligands with high affinity and selectivity for the histamine H_2 receptor. *J Med Chem* **35:**2231–2238.

Hough LB (2001) Genomics meets histamine receptors: new subtypes, new receptors. *Mol Pharmacol* **59:**415–419.

Isogaya M, Sugimoto Y, Tanimura R, Tanaka R, Kikkawa H, Nagao T, and Kurose H (1999) Binding pockets of the β_1- and β_2-adrenergic receptors for subtype-selective agonists. *Mol Pharmacol* **56:**875–885.

Kopin AS, McBride EW, Schaffer K, and Beinborn M (2000) CCK receptor polymorphisms: an illustration of emerging themes in pharmacogenomics. *Trends Pharmacol Sci* **21:**346–353.

Ligneau X, Morisset S, Tardivel-Lacombe J, Gbahou F, Ganellin CR, Stark H, Schunack W, Schwartz JC, and Arrang JM (2000) Distinct pharmacology of rat and human histamine H_3 receptors: role of two amino acids in the third transmembrane domain. *Br J Pharmacol* **131:**1247–1250.

Liu H-Y, Wenzel-Seifert K, and Seifert R (2001) The olfactory G-protein $G_{\alpha olf}$ possesses a lower GDP-affinity and deactivates more rapidly than $G_{s\alpha short}$: Consequences for receptor-coupling and adenylyl cyclase activation. *J Neurochem* **78:**325–338.

Lovenberg TW, Pyati J, Chang H, Wilson SJ, and Erlander MG (2000) Cloning of rat histamine H_3 receptor reveals distinct species pharmacological profiles. *J Pharmacol Exp Ther* **293:**771–778.

Milligan G (2000) Insights into ligand pharmacology using receptor-G-protein fusion proteins. *Trends Pharmacol Sci* **21:**24–28.

Nederkoorn PH, van Gelder EM, Donne-Op den Kelder GM, and Timmerman H (1996) The agonistic binding site at the histamine H_2 receptor. II. Theoretical investigations of histamine binding to receptor models of the seven alpha-helical transmembrane domain. *J Comput Aided Mol Des* **10:**479–489.

Palczewski K, Kumasaka T, Hori T, Behnke CA, Motoshima H, Fox BA, Le Trong I, Teller DC, Okada T, Stenkamp RE, et al. (2000) Crystal structure of rhodopsin: A G protein-coupled receptor. *Science (Wash DC)* **289:**739–745.

Schalkhausser F (1998) *Solution and Solid Phase Synthesis of Non-Symmetrically Substituted Guanidines: Preparation and Pharmacological Activity of New Highly Potent Histamine H_2 Receptor Agonists*. PhD thesis, University of Regensburg, Regensburg, Germany.

Schuster A, Bernhardt G, and Buschauer A (1997) Determination of the arpromidine-type histamine H_2-receptor agonist. N^1-[3–3,4-difluorophenyl)-3–2(2-pyridyl)propyl]-N^2-[3-(1*H*-imidazol-4-yl)propyl]guanidine and corresponding N^3-alkoxycarbonylguanidines by HPLC and CE. *Eur J Pharmaceut Sci* **5:**79–88.

Seifert R, Höer A, Schwaner I, and Buschauer A (1992) Histamine increases cytosolic Ca^{2+} in HL-60 promyelocytes predominantly *via* H_2 receptors with an unique agonist/antagonist profile and induces functional differentiation. *Mol Pharmacol* **42:**235–241.

Seifert R, Lee TW, Lam VT, and Kobilka BK (1998a) Reconstitution of β_2-adrenoceptor-GTP-binding-protein interaction in Sf9 cells: High coupling efficiency in a β_2-adrenoceptor-$G_{s\alpha}$ fusion protein. *Eur J Biochem* **255:**369–382.

Seifert R, Wenzel-Seifert K, Gether U, and Kobilka BK (2001) Functional differences between full and partial agonists: Evidence for ligand-specific receptor conformations. *J Pharmacol Exp Ther* **297:**1218–1226.

Seifert R, Wenzel-Seifert K, and Kobilka BK (1999) GPCR-G_α fusion proteins: an approach for the molecular analysis of receptor/G-protein coupling. *Trends Pharmacol Sci* **20:**383–389.

Seifert R, Wenzel-Seifert K, Lee TW, Gether U, Sanders-Bush E, and Kobilka BK (1998b) Different effects of $G_s\alpha$ splice variants on β_2-adrenoreceptor-mediated signaling. The β_2-adrenoreceptor coupled to the long splice variant of $G_s\alpha$ has properties of a constitutively active receptor. *J Biol Chem* **273:**5109–5116.

Traiffort E, Vizuete ML, Tardivel-Lacombe J, Souil E, Schwartz JC, and Ruat M (1995) The guinea pig histamine H_2 receptor: gene cloning, tissue expression and chromosomal localization of its human counterpart. *Biochem Biophys Res Commun* **211:**570–577.

MOL PHARM
MOLECULAR PHARMACOLOGY
aspet
Downloaded from molpharm.aspetjournals.org by guest on December 1, 2012

Wenzel-Seifert K and Seifert R (2000) Molecular analysis of β_2-adrenoceptor coupling to G_s-, G_i-, and G_q-proteins. *Mol Pharmacol* **58:**954–966.
Wenzel-Seifert K, Arthur JM, Liu HY, and Seifert R (1999) Quantitative analysis of formyl peptide receptor coupling to $G_i\alpha_1$, $G_i\alpha_2$, and $G_i\alpha_3$. *J Biol Chem* **274:**33259–33266.
Wieland K, Zuurmond HM, Krasel C, Ijzerman AP, and Lohse MJ (1996) Involvement of Asn-293 in stereospecific agonist recognition and in activation of the β_2-adrenergic receptor. *Proc Natl Acad Sci USA* **93:**9276–9281.
Wieland K, Laak AM, Smit MJ, Kühne R, Timmerman H, and Leurs R (1999) Mutational analysis of the antagonist-binding site of the histamine H_1 receptor. *J Biol Chem* **274:**29994–30000.

Address correspondence to: Dr. Roland Seifert, Department of Pharmacology and Toxicology, The University of Kansas, 5064 Malott Hall, Lawrence, KS 66045. E-mail: rseifert@ukans.edu

MOL PHARM
MOLECULAR PHARMACOLOGY
aspet
Downloaded from molpharm.aspetjournals.org by guest on December 1, 2012